

**APPLYING AND ANALYZING ROBUST  
MODERN CONTROL ON UNCERTAIN  
HYDRAULIC SYSTEMS**

---

A thesis presented to the faculty of the Graduate School  
University of Missouri-Columbia

---

In Partial Fulfillment  
Of the Requirements for the Degree  
Master of Science

---

By

**BRIAN BAX**

Dr. Roger Fales, Thesis Supervisor

May 2006

The undersigned, appointed by the dean of the Graduate School, have examined the project entitled

**APPLYING AND ANALYZING ROBUST  
MODERN CONTROL ON UNCERTAIN  
HYDRAULIC SYSTEMS**

Presented by Brian Bax

a candidate for the degree of Masters of Science

and hereby certify that in their opinion it is worthy of acceptance.

---

Dr. Roger Fales, Assistant Professor, Mechanical and Aerospace Engineering

---

Dr. Craig Kluever, Professor, Mechanical and Aerospace Engineering

---

Dr. Steven Borgelt, Associate Professor, Biological Engineering

## ACKNOWLEDGEMENTS

Though not always the easiest endeavor, attending graduate school at the University of Missouri-Columbia has been an adventure. And like all adventures, there has been joy, excitement, discovery and many times when the phrase “I don’t know if I’m going to make it out alive” has been uttered. It would have never been possible without the help and guidance given to me by friends and along the way.

I am especially thankful to my academic advisor, Dr. Roger Fales for his patience, aid and faith in me throughout my graduate experience. Had Dr. Fales not offered me the support and help he has over the past year and a half, none of this would have been possible.

I am also thankful for Dr. Kluever who has guided me through many dynamics and control classes throughout my tenure at the university as both an undergraduate and graduate and for agreeing to serve on my thesis committee.

I express my thanks to Dr. Borgelt for his willingness to find the time to read my thesis and participate on my thesis committee.

I thank Dr. Manring for sparking my interest in hydraulics and giving me the opportunity to do undergraduate research under him which inevitably caused me to attend graduate school.

I am also thankful for my colleague Patrick Dean for his hard work and support on this research project.

Last, but certainly not least, I’d like to thank my parents, Fred and Brenda, my sister, Megan, my friends and family for their endless love and support in all things in life both near and far to academia.

## TABLE OF CONTENTS

Acknowledgements.....	ii
List of Figures.....	vi
List of Tables.....	viii
Nomenclature.....	ix
Abstract.....	x
<b>Chapter 1 – Introduction .....</b>	<b>1</b>
1.1 – PID Limitations.....	2
1.2 – Modern Control in Hydraulic systems.....	3
1.3 – Research Objectives.....	3
1.4 – Thesis Outline .....	4
<b>Chapter 2 – IMV Hydraulic System Modeling .....</b>	<b>5</b>
2.1 – First Principle Modeling .....	5
2.2 – Nonlinear Model Validation .....	8
2.3 – Linearization and Validation.....	12
2.4 – Categorizing and Modeling System Uncertainty.....	19
<b>Chapter 3 – <math>H_{\infty}</math> Control Mechanisms.....</b>	<b>24</b>
3.1 – Necessity of $H_{\infty}$ Control Routines.....	24
3.2 – The $H_{\infty}$ Control Problem.....	24
3.3 – Mixed Sensitivity $H_{\infty}$ Control.....	27
3.4 – MacFarlane-Glover $H_{\infty}$ Loop-shaping.....	29
3.5 – Two Degrees-of-Freedom $H_{\infty}$ Control.....	31
<b>Chapter 4 – Application of Control Routines.....</b>	<b>34</b>

4.1 – Performance Requirements .....	34
4.2 – Baseline PID Design .....	35
4.3 – Mixed Sensitivity Design – Application.....	39
4.4 – MacFarlane-Glover $H_\infty$ Loop-shaping – Application .....	42
4.5 – Two Degrees-of-Freedom $H_\infty$ Control - Application.....	47
<b>Chapter 5 – Time Domain Analysis of Robustness.....</b>	<b>54</b>
5.1 – Uncertainty Cases .....	54
5.2 – Time Domain Responses .....	54
5.3 – Time Domain Analysis Conclusions .....	61
<b>Chapter 6 – Frequency Domain Analysis of Robustness .....</b>	<b>62</b>
6.1 – Frequency Domain Robustness Principles.....	62
6.2 – Applying Robust Analysis to PID.....	64
6.3 – Applying Robust Analysis to Mixed Sensitivity Control .....	65
6.4 – Applying Robust Analysis to MacFarlane-Glover $H_\infty$ Loop-shaping Control .....	67
6.5 – Applying Robust Analysis to Two Degrees-of-Freedom $H_\infty$ Loop-shaping Control .....	68
6.6 – Robustness Conclusions .....	69
<b>Chapter 7 – Conclusions.....</b>	<b>71</b>
7.1 – Overview.....	71
7.2 – Limitation of $H_\infty$ Control .....	72
7.3 – Scope of Future Work.....	72
<b>Appendices.....</b>	<b>73</b>

A – Matlab Code for Mixed Sensitivity.....	73
B – Matlab Code for MacFarlane-Glover Loop-shaping.....	77
C – Matlab Code for Two Degrees-of-Freedom Loop-shaping.....	80
D – Creating the Generalized Plant, P, for Robustness Analysis .....	85
<b>References .....</b>	<b>88</b>

## LIST OF FIGURES

1)	Fig. 2.1.1 – A schematic for the IMV system model.....	5
2)	Fig. 2.1.2 – The internal mechanical feedback of the variable displacement pump .....	7
3)	Fig. 2.2.1 – Data validation for pump displacement.....	9
4)	Fig. 2.2.2 – Data validation for cylinder position.....	10
5)	Fig. 2.2.3 – Data validation for cylinder head-end pressure.....	11
6)	Fig. 2.3.1 – Linear model validation for cylinder velocity .....	14
7)	Fig. 2.3.2 – Linear model validation for head-end pressure .....	15
8)	Fig. 2.3.3 – Pole-zero map of the linearized system.....	16
9)	Fig. 2.3.4 – Singular value plot for the linearized system .....	18
10)	Fig. 2.4.1 – Output multiplicative uncertainty.....	22
11)	Fig. 2.4.2 – Output uncertainty transfer function.....	23
12)	Fig. 3.2.1 – The generalized plant model.....	25
13)	Fig. 3.3.1 – One degree-of-freedom feedback configuration.....	27
14)	Fig. 3.3.2 – S/KS form of MS for tracking .....	29
15)	Fig. 3.5.1 – Two degrees-of-freedom design schematic.....	32
16)	Fig. 4.2.1 – Margin pressure step response for linear PID .....	36
17)	Fig. 4.2.2 – Velocity step response for linear PID.....	36
18)	Fig. 4.2.3 – Margin pressure response for PID control on the nonlinear model .....	37
19)	Fig. 4.2.4 – Velocity response for PID control on the nonlinear model.....	38

20)	Fig. 4.3.1 – Margin pressure step response for linear mixed sensitivity .....	40
21)	Fig. 4.3.2 – Velocity step response for linear mixed sensitivity.....	40
22)	Fig. 4.3.3 – Margin pressure response for mixed sensitivity control on the nonlinear model .....	41
23)	Fig. 4.3.4 – Velocity response for mixed sensitivity control on the nonlinear model.....	42
24)	Fig. 4.4.1 – Control schematic for MacFarlane-Glover control .....	43
25)	Fig. 4.4.2 – Margin pressure step response for linear MacFarlane-Glover .....	44
26)	Fig. 4.4.3 – Velocity step response for linear MacFarlane-Glover.....	44
27)	Fig. 4.4.4 – Margin pressure response for MacFarlane-Glover control on the nonlinear model .....	45
28)	Fig. 4.4.5 – Velocity response for MacFarlane-Glover control on the nonlinear model.....	46
29)	Fig. 4.5.1 – Step response of the desired closed-loop transfer function matrix .....	48
30)	Fig. 4.5.2 – Margin pressure step response for linear 2 degrees-of-freedom control .....	49
31)	Fig. 4.5.3 – Velocity step response for linear 2 degrees-of-freedom control .....	49
32)	Fig. 4.5.4 – Margin pressure response for 2 degrees-of-freedom control on the nonlinear model .....	50
33)	Fig. 4.5.5 – Velocity response for 2 degrees-of-freedom control on the nonlinear model.....	51
34)	Fig. 4.5.6 – PZ-map for 2 degrees-of-freedom controller prior to reduction.....	52



35)	Fig. 4.6.7 – PZ-map for 2 degrees-of-freedom controller post reduction.....	53
36)	Fig. 5.2.1 – Margin pressure robustness for PID control.....	55
37)	Fig. 5.2.2 – Velocity robustness for PID control .....	55
38)	Fig. 5.2.3 – Margin pressure for the MS controller .....	56
39)	Fig. 5.2.4 – Velocity robustness for MS controller.....	57
40)	Fig. 5.2.5 – Margin pressure robustness for MG controller.....	58
41)	Fig. 5.2.6 – Velocity robustness for MG controller .....	58
42)	Fig. 5.2.7 – Margin pressure robustness for 2DOF controller .....	59
43)	Fig. 5.2.8 – Velocity robustness for the 2DOF controller .....	60
44)	Fig. 6.1.1 – Transforming P and K into the N- $\Delta$ structure .....	63
45)	Fig. 6.2.1 – Robustness analysis for PID controller .....	65
46)	Fig. 6.3.1 – Robustness analysis for mixed sensitivity controller .....	66
47)	Fig. 6.4.1 – Robustness analysis for MacFarlane-Glover $H_\infty$ loop-shaping control .....	67
48)	Fig. 6.5.1 – Robustness analysis for two degrees-of-freedom $H_\infty$ loop-shaping control .....	68

### LIST OF TABLES

1)	Table 2.4.1 – Uncertain Characteristics in the IMV hydraulic system.....	20
2)	Table 2.4.2 – Range of variance for the system’s parameters .....	21
3)	Table 4.4.1 – Performance requirements for velocity and margin pressure control .....	34
4)	Table 6.6.1 – Summary for frequency domain robustness analysis .....	69

## NOMENCLATURE

Symbol	Description	Units
$P_p$	Pump pressure	Pa
$P_A$	Head-end pressure	Pa
$P_B$	Rod-end pressure	Pa
$P_c$	Control Pressure (within the pump)	Pa
$P_T$	Tank pressure	Pa
$Q_{1,2,3,4}$	Flow through each valve	$m^3/sec$
$V_A$	Volume in head-end of cylinder	$m^3$
$V_B$	Volume in rod-end of cylinder	$m^3$
$V_C$	Volume of displacement control cylinder	$m^3$
$A_A$	Head-end area	$m^2$
$A_B$	Rod-end area	$m^2$
$A_C$	Control cylinder area	$m^2$
$k$	Flow equation constant	$[m^3/kg]^{1/2}$
$\rho$	Fluid density	$kg/m^3$
$y$	Cylinder position	m
$y_{max}$	Maximum cylinder position	m
$m$	Mass of the cylinder and bucket	kg
$F$	Bias Force	N
$c$	Damping coefficient	N/m/s
$b$	Pump damping coefficient	N/m/s
$J_{eff}$	Pump moment of inertia	$Nms^2$
$\theta$	Pump angular position	Radians
$D_p$	Pump displacement	$M^3$
$\beta$	Fluid bulk modulus	GPa
$C_d$	Discharge coefficient	-
$z$	Displacement control cylinder position	m
$x$	Pump spool valve displacement	m
$T_C$	Torque from displacement control valve	Nm
$T_L$	Torque imparted from pressure in the pump	Nm
$\omega_p$	Pump speed	rad/s
$K_l$	Leakage in the pump	$m^3/s/Pa$

## ABSTRACT

In this work modern robust control systems are designed and compared to standard techniques for a hydraulic implement system. The system includes an independent metering valve (IMV) and a variable displacement pump. The IMV is a powerful and versatile valve assembly. The IMV's inherent complexity makes classic control methods difficult to design. Parameter variations and unmodeled dynamics can cause sluggish performance and instability in some cases. By applying modern control, robustness can be improved relative to classical and single-input/single-output (SISO) control design techniques. Techniques such as  $H_\infty$  control have been proven effective in many multiple-input/multiple-output (MIMO) applications. Linear analysis shows improvement in robustness characteristics of the IMV system over a conventional PID control scheme. Nonlinear simulations show favorable system response and similarly positive robustness traits for the modern control designs.

## Chapter 1

### INTRODUCTION

Control systems need to operate under a variety of conditions. Therefore, the design process for a controller includes considerations of less than ideal conditions of operation. Traditionally, a controller is designed with some stability margin and then tested or simulated under conditions which the controller is expected to see. This typically involves some trial and error between control redesign and model simulations. Modern control design techniques allow a designer to more easily develop a control system which will work in cases where the machine may be worn or manufactured in an unexpected way. Therefore, modern control design techniques can be used to improve the reliability of machines since the control system will continue to operate over a wide range of adverse conditions.  $H_\infty$  control design techniques make it easier to get higher performance than traditional techniques. Design of  $H_\infty$  controllers involves shaping the maximum singular value of specified transfer functions over specific frequencies.  $H_\infty$  techniques also employ optimization and have more flexibility in terms of balance between performance and stability.

Hydraulic systems are a good application for modern robust control design techniques. Robustness is a measure of system's ability to produce uniform performance and stability results under varying conditions. Hydraulic systems tend to be designed with conservative performance since stability is a concern. A more advanced controller may improve performance and stability robustness at the same time especially in the case

of multiple input, multiple output (MIMO) systems. A number of hydraulic systems could be considered for robustness analysis and  $H_\infty$  control design which could improve stability and performance. An independent metering valve (IMV) hardware setup is a good application for robust control design using  $H_\infty$  methods since the system has multiple inputs and outputs and model uncertainty. Since the system has coupled dynamics, it is likely that a MIMO approach to control design will improve performance and robustness over single input single output (SISO) design techniques, such as proportional, integral and derivative control (PID).

### **1.1 PID Limitations**

The difficulty that arises from SISO control lies in the way different inputs and outputs pairs are coordinated. As seen in Zhang et. al [1] for a system with  $m$  inputs and  $n$  outputs,  $m \times n$  individual PID controllers have to be tuned for each input-output couple. Furthermore, Zhang continues by explaining that if each controller has to consider the others, more knowledge about the system is needed and it is harder to achieve robust performance. Skogestad and Postlethwaite [2] further this argument by explaining that stacking PID controllers in an effort to emulate MIMO control often leads to erroneous robustness analysis results. SISO systems tend to show robust performance when nominal performance and robust stability are satisfied. However, this is not true for MIMO systems. So, stacking together SISO controls robustness analysis can be duped into showing robust performance where it would not truly exist. For this system, PID control would result in these stacked SISO controllers that would tend to show false robustness results.

## **1.2 Modern Control in Hydraulic Systems**

Unfortunately, there are few examples of modern control MIMO techniques that have been applied to hydraulic systems. Active application of  $H_\infty$  control has been done by Zhang et. al [1] on hydraulic powertrains for earthmoving vehicles. The results of this research showed that  $H_\infty$  provided the ability to robustly control the hydraulic powertrain. In the application of active hydraulic suspension explored by Chen et. al [3] it was shown that  $H_\infty$  control could be successfully implemented. They also examined robustness characteristics of  $H_\infty$  control and found favorable results. Fales et. al [4, 5] showed that modern control could be applied successfully to a double inverted pendulum that was regulated by hydraulic actuators. However, the most applicable research comes from Fales and Kelkar [6] who applied mixed-sensitivity  $H_\infty$  control to regulate the bucket of a front wheel loader. This research successfully showed through robustness analysis that the controller was successful in withstanding plant perturbations.

## **1.3 Research Objectives**

The specific objectives of this research are to accurately model an IMV hydraulic system through nonlinear and linear analysis, examine  $H_\infty$  control routines with increased robustness characteristics, apply the  $H_\infty$  control routines and to analyze their responses in both the time and frequency domain.

## 1.4 Thesis Outline

Chapter 2 discusses the modeling of the IMV hydraulic system from first principle model through validation, linearization and linear analysis. Uncertainty modeling is also examined. Chapter 3 discusses the theory and need for each modern controller to be examined. The theoretical background is important to know where robust design comes from and why they are needed. Also, methods of application are discussed. Chapter 4 deals with applying the specific controllers to the system. The performance weighting is defined and each controller is examined in the time domain on the nominal model. Comparisons are drawn between the linear and nonlinear responses for each controller. In Chapter 5, time domain robustness is examined for the controllers. Each controller is applied to two separate perturbation bias cases and the resulting responses are examined to determine relative robustness. Chapter 6 deals with robustness analysis in the frequency domain. The theory behind robustness analysis is discussed and applied to each control routine. This analysis gives a way to compare the control routines through numerical methods. Finally, Chapter 7 contains overall conclusions about the research, discusses limitations to  $H_\infty$  control and proposes future work.

## Chapter 2

### IMV Hydraulic System Modeling

#### 2.1 First Principle Modeling

The IMV system, as seen in the schematic in Fig. 2.1.1, is a connection of four variable valve assemblies, a variable displacement pump and a single-rod hydraulic cylinder. Modeling techniques used throughout this section can be found in Manning [7]. Please refer to the nomenclature section for variable names.

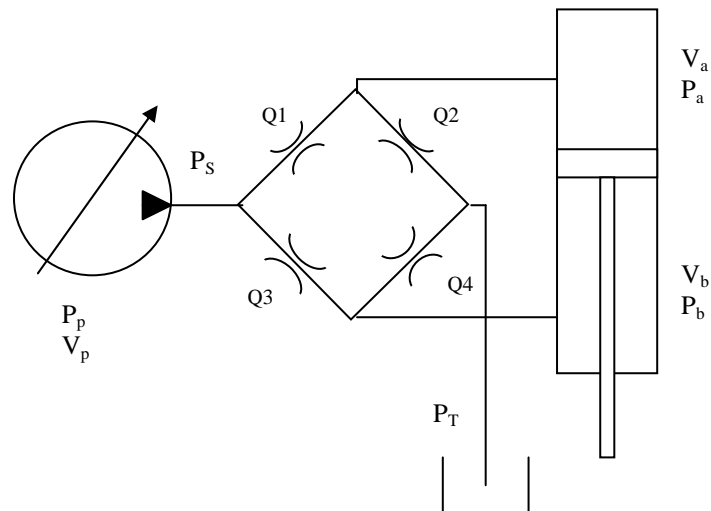


**Fig 2.1.1 – A schematic of the IMV system modeled**

Modeling began with the pressure rise rates associated with each side of the cylinder. This modeling was done by using the summation of flow into and out of each side, fluid bulk modulus, volume of each side of the cylinder and volume change rates for each side. The respective pressure rise rates for both the A, head side, and B, rod side, can be seen as:



$$\dot{P}_A = \frac{\beta}{V_A} (-Q_2 + Q_1 - \dot{V}_A), \quad (2.1.1)$$

$$\dot{P}_B = \frac{\beta}{V_B} (-Q_4 + Q_3 - \dot{V}_B). \quad (2.1.2)$$

The flow for each side of the cylinder is directed from each valve, which can be identified by their respective numbering. The volumetric flow rate,  $Q$ , is modeled using the classical orifice equation which is based on the Bernoulli equation.

$$Q_i = kA_i \sqrt{P_S - P_A}. \quad (2.1.3)$$

This flow equation utilizes the pressure drop across each valve, the valve area and includes the constant  $k$ , which is defined as:

$$k = C_d \sqrt{\frac{2}{\rho}}. \quad (2.1.4)$$

The volumes and volume rise rates for each cylinder side were modeling via geometry:

$$V_A = A_A y + V_O, \quad (2.1.5)$$

$$V_B = A_B (y_{\max} - y) + V_O, \quad (2.1.6)$$

$$\dot{V}_A = A_A \dot{y}, \quad (2.1.7)$$

$$\dot{V}_B = -A_B \dot{y}. \quad (2.1.8)$$

Cylinder load dynamics were modeled using standard linear dynamics including viscous drag in the cylinder but not including a spring effect balancing with the forces resulting from pressurizing each side. The equation of motion follows:

$$m\ddot{y} + c\dot{y} = P_A A_A - P_B A_B + F \quad (2.1.9)$$

The force,  $F$ , is a bias force nominally set to zero. It should be noted that this model does not account for leakage between the two volumes.

The variable displacement pump used for this project is a complex pump with significant internal dynamics. The pump has internal mechanical feedback that requires modeling whose schematic can be seen in Figure 2.1.2.

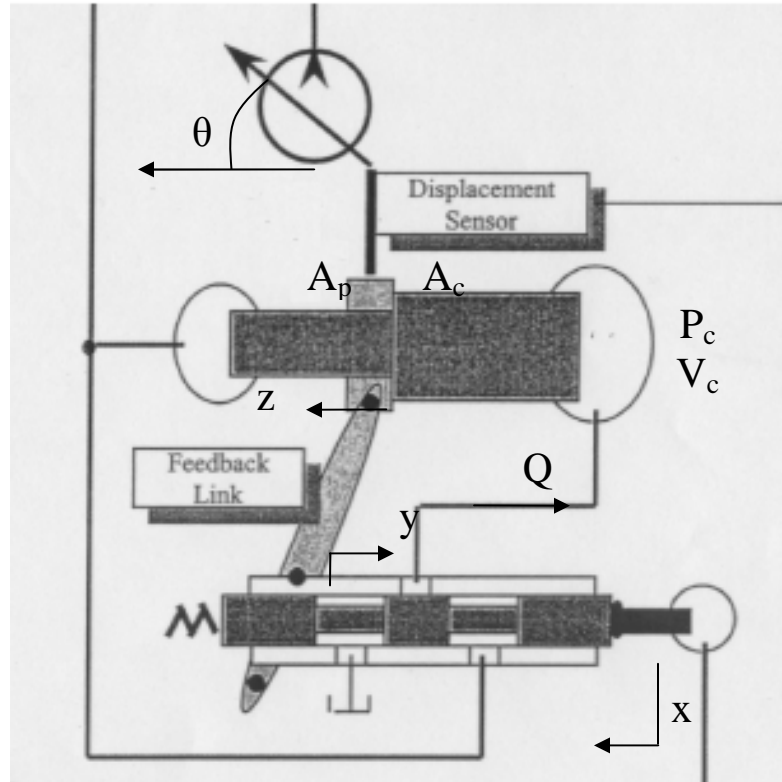


**Fig. 2.1.2 – The internal mechanical feedback of the variable displacement pump [8]**

$P_c$  is the pressure on one end of the displacement control cylinder. The pressure rise rate is as follows:

$$\dot{P}_c = \frac{\beta}{V_c} (Q_c - \dot{z}A_c) \quad (2.1.10)$$

The volumetric flow rate in the pump is modeled using the classical orifice equation:

$$Q_c = C_d k (x - y) \sqrt{\frac{\rho}{2} (P_p - P_c)} \quad (2.1.11)$$

The equation of motion for the swash plate angle is:

$$J_{eff} \ddot{\theta} + b \dot{\theta} = T_C - T_L \quad (2.1.12)$$

where  $T_L$  is the torque imparted from the pressure in the pump cylinders and  $T_C$  is the torque from the actuator cylinder. The discharge pressure of the pump, which is the supply pressure identified in other parts of the model, is calculated as the pressure rise rate in the discharge volume,  $V_p$ , as follows:

$$\dot{P}_p = \frac{\beta}{V_p} (\omega_p D_p(\theta) - Q_1 - Q_3 - K_l P_p). \quad (2.1.13)$$

where it should be noted that leakage is taken into account and  $D_p$  is a function of  $\theta$ . Also of note, only flows 1 and 3 are modeled here because only these two valves are being used for control. This system feature will be covered in greater detail later.

The model of the valve actuators were found by fitting transfer functions and look-up tables to experimental data. The transfer functions modeled current drivers in the system and the look-up tables related input current to output valve area. Also, hysteresis effects were taken into account so that the relationships present in the matching test data were present in the simulation of the model.

## 2.2 Nonlinear Model Validation

The model used for design has some shortcomings; certain system parameters were not included and some subsystems were considered ideal. These assumptions were made for the sake of keeping an already complex model from becoming too complex to use. Also, because robust design techniques were being used, some system model errors can be accounted for by robustness analysis and design. Unmodeled parameters include pump efficiencies and cross-cylinder leakage. Also, constant engine speed and torque were assumed. Orifice flow and pressure compensators are both considered ideal.

Despite unmodeled dynamics and idealized components, the nonlinear system model matched test data remarkably well. Figure 2.2.1 shows a comparison between experimental data and simulation data for pump displacement.

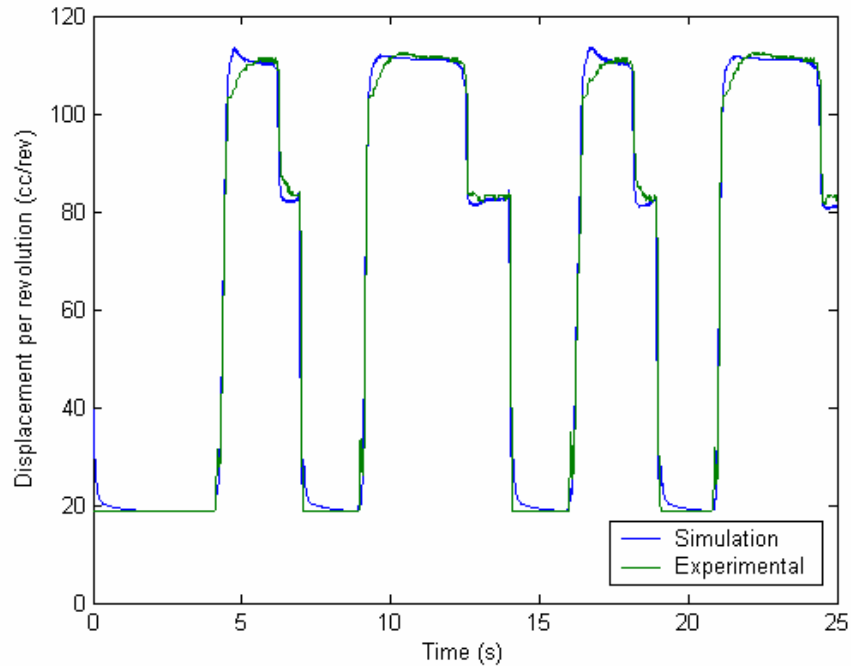


**Fig 2.2.1 – Data validation for pump displacement [8]**

From Figure 2.2.1, it can be seen that the simulation matched very well with the experimental data. Discrepancies exist at the start of the upward step responses but the severity of error is not extreme. The simulation quickly returns to match the experimental results. Also, the simulation closely matches the downward step responses seen on the backside of the square wave signal. Figure 2.2.2 shows a comparison between experimental data and simulation data for cylinder position.

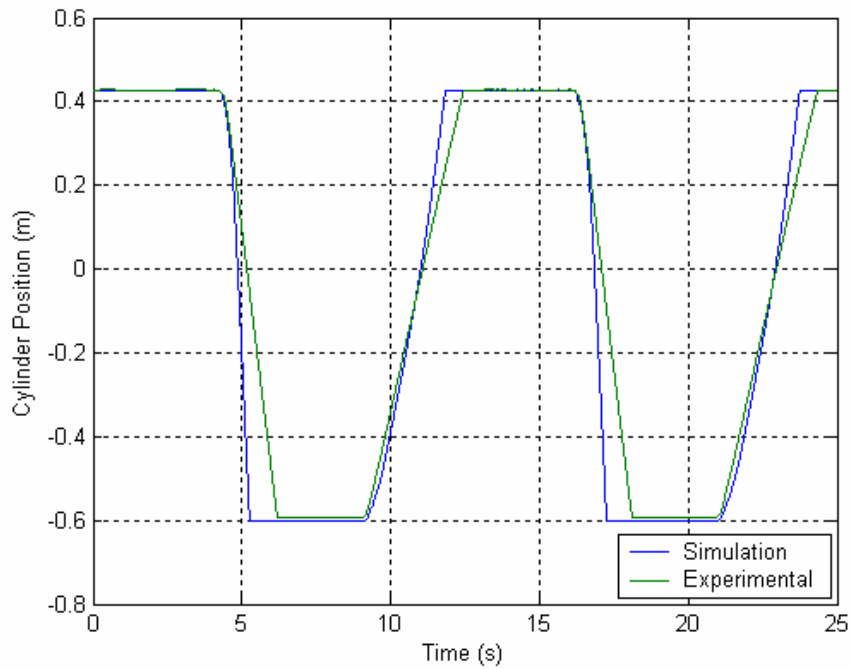


**Fig. 2.2.2 – Data validation for cylinder position [8]**

From Figure 2.2.2, it can be seen that the simulation matches the experimental data somewhat accurately. The slope differences present in the comparison is due to unmodeled cross-cylinder leakage. If leakage had been modeled, less pressure would be on the high pressure side of the cylinder causing the cylinder to move more slowly. It can be seen that the simulation cylinder does indeed move faster than the experimental. Figure 2.2.3 shows a comparison between experimental data and simulation data for head-end pressure.

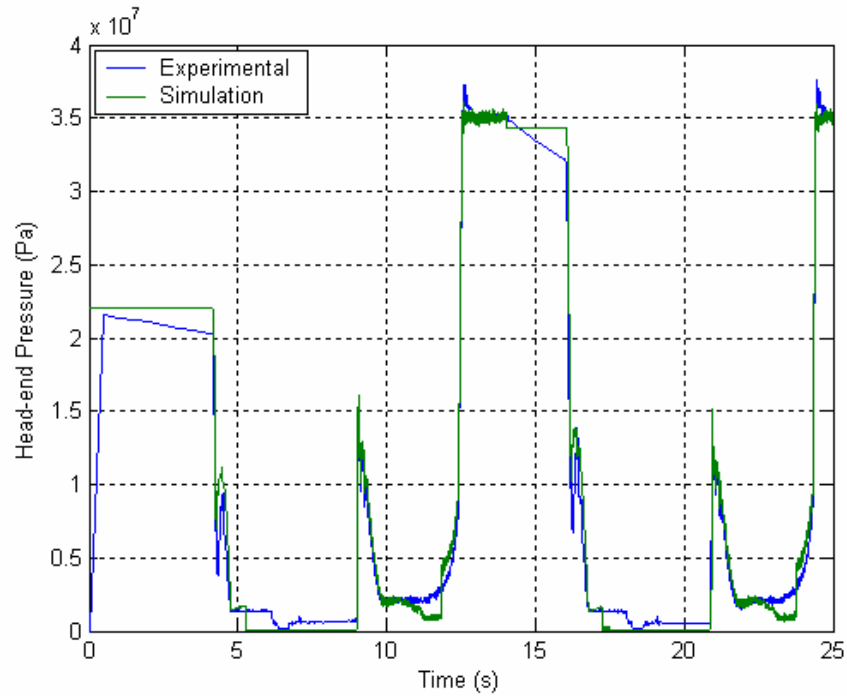


**Fig. 2.2.3 – Data validation for cylinder head-end pressure [8]**

From Figure 2.2.3 it can be seen that simulation matches the experimental data very closely. The model simulation closely follows the dynamics found in the pressure response, but once again the unmodeled leakage can be seen, specifically in the time spanning 0-5 seconds and 12-17 seconds. It can be seen that in the experimental data, the pressure drops over periods where simulated pressure is constant. This is the effect of leakage causing the pressure to drop over time. Leakage aside, the simulation closely matches the experiments in all cases but the low pressure settling (below 5 MPa).

Overall, these modeling errors are acceptable due to the ability of the controllers to account for levels of uncertainty and inaccuracy. Also, these inaccuracies can be encompassed in uncertainty analysis that will be presented later.

## 2.3 Linearization and Validation

Linearization of the systems is typically done by examining the Taylor Series expansion of a system about an operation point. This method was inconvenient in this case because of the way the valve dynamics were modeled. The look-up table format did not allow for proper differentiation. Instead a finite-differencing method was used to linearize the system. This process was carried out by my colleague in [8]. The finite-differencing method of linearization is a numerical method for building the system matrices of a model. By perturbing each state minutely from their nominal and then observing the state-vector response, the system matrices were constructed in turn. This result is derived by using the approximation:

$$\frac{\partial f_n}{\partial x_m} \approx \frac{\Delta f_n}{\Delta x_m} = \frac{f_{n,nom} - f_{n,perturb\_x_m}}{x_{m,nom} - x_{m,perturbed}} \quad (2.3.1)$$

where  $n$  is the number of each function of the system and  $m$  is the number of each state of the system. Nominal values used for this system are the system values at the mid-stroke of the cylinder. Through Eq (2.3.1) each individual element of the  $A$  and  $B$  matrices could be found. The system matrices were calculated by using:

$$\underline{\underline{A}} = \begin{bmatrix} \frac{\partial f_1}{\partial x_1} & \frac{\partial f_1}{\partial x_2} & \dots \\ \frac{\partial f_2}{\partial x_1} & \frac{\partial f_2}{\partial x_2} & \dots \\ \vdots & \vdots & \ddots \end{bmatrix} \quad (2.3.2)$$

$$\underline{\underline{B}} = \begin{bmatrix} \frac{\partial f_1}{\partial u_1} & \frac{\partial f_1}{\partial u_2} & \dots \\ \frac{\partial f_2}{\partial u_1} & \frac{\partial f_2}{\partial u_2} & \\ \vdots & & \ddots \end{bmatrix} \quad (2.3.3)$$

The final linearized model consists of 16 states:

$$\bar{x} = [\theta \quad \dot{\theta} \quad P_c \quad P_p \quad P_A \quad P_B \quad y \quad \dot{y} \quad x_1 \quad \dots \quad x_8]^T \quad (2.3.4)$$

with two inputs and two outputs. In Eq. (2.3.4),  $x_n$  represents the states of each valve assembly and current amplifier involved in the IMV system. The measurements of the system are the load velocity and the margin pressure.

$$\bar{y} = [(P_p - P_A) \quad \dot{y}]^T \quad (2.3.5)$$

Margin pressure is defined as the pressure drop across the valve. In other words, margin pressure is the difference between pump pressure and head-end pressure. The two inputs to the system are the commanded pump displacement and a single valve input.

$$\bar{u} = [D_p \quad i_{1,4}]^T \quad (2.3.6)$$

Current  $i_{1,4}$ , is for both the first and fourth valve, which lead to the pump-to-cylinder head-end valve and the cylinder-to-tank rod-end valve respectively. These two valves are slaved together at a 1:1 ratio for the sake of ease in control design. Valves two and three are not used for control and remain closed for all time.

In similar fashion to the nonlinear model, the linearized model was validated via comparison, but this time to the nonlinear model. Two individual states were analyzed: load velocity and cylinder head-end pressure. Each model was given a step input and the



results were over-plotted. In Figure 2.3.1, the comparison of cylinder velocity can be seen.

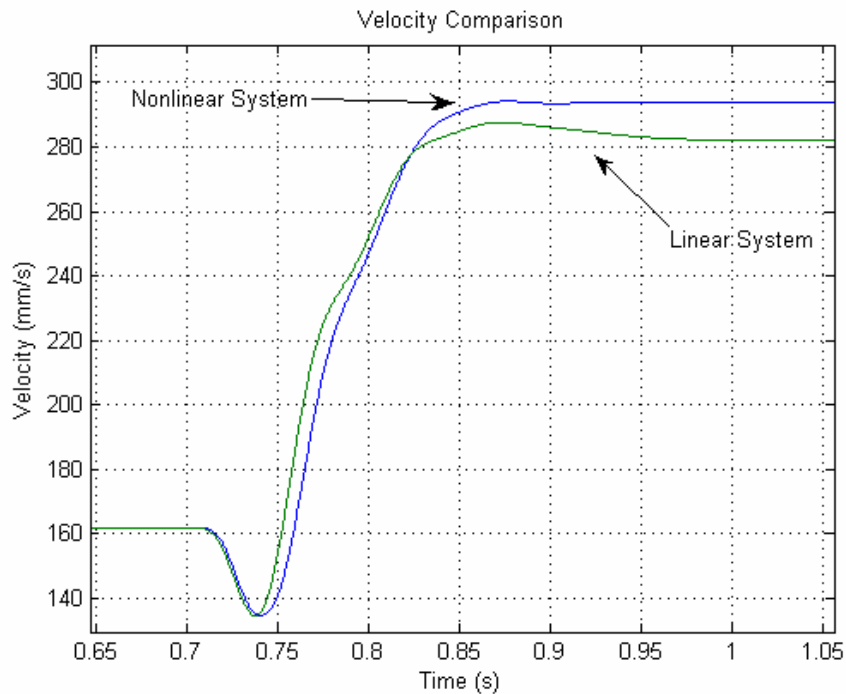


**Fig. 2.3.1 – Linear model validation for cylinder velocity [8]**

From Figure 2.3.1 it can be seen that the linear model accurately replicates the non-minimum phase response present in the nonlinear model. It should be noted that this non-minimum phase response is due to the current drivers present in the valves. Figure 2.3.1 also shows that the linear system shows similar dynamic responses to the nonlinear model though showing an increased steady-state error. Figure 2.3.2 shows the comparison of head-end pressures for the linear and nonlinear model for a step input.

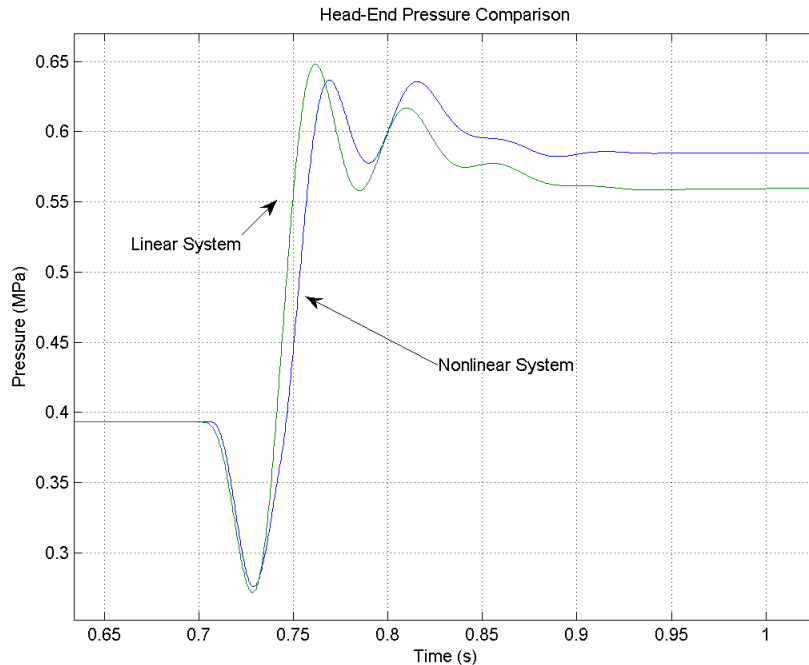


**Fig. 2.3.2 – Linear model validation for head-end pressure [8]**

In Figure 2.3.2, it can be seen that the linear model matches the nonlinear model fairly accurately. The same non-minimum phase dynamics is present in both data sets and similar dynamic responses are also present. Here too, however, the increased steady-state error is also present. The discrepancies found in both comparisons will be accounted for in the modeling of system uncertainty and the application of robust control schemes and should not cause a problem in practical application. However, uncertainty and model mismatching is to be expected. As a linearized system strays from its linearized point, the system is less accurate. The mismatching occurring between the linearized model and the nonlinear model could very well be due to the fact that the linearized system varies from its linearization point, which was mid stroke, during the dynamic response imparted by the step input.

To further analyze the linear system, two analysis tools were used to evaluate the system: pole-zero maps and singular value plots. The pole-zero map of the final 16-state system can be seen in Figure 2.3.3. It is apparent from this graph that the system is stable because all poles of the system lie in the left-half plane.

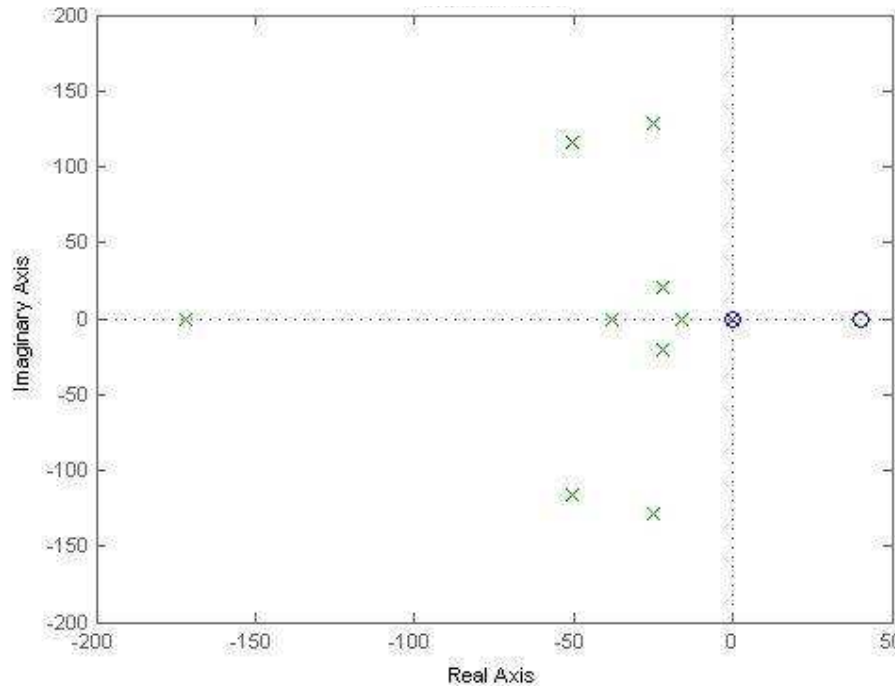


**Fig. 2.3.3 – Pole-zero map of the linearized system [8]**

However, the pole-zero map in Figure 2.3.3 does show a system zero in the right-half plane. For stability, a right-half zero does not represent the inherent instability that a right-half pole would. A right-half plane zero merely represents a performance limitation in the system. In this case, with a pure-real zero at positive 40 rad/sec, it causes a bandwidth limitation equal to approximately 3 Hz for the closed-loop system [2]. This bandwidth limitation applies to any effort to design a control system with a bandwidth past that threshold. The presence of a right-half plane zero does support the findings of non-minimum phase behavior in the experimental data. Through inspection of the

system, it was found that the right-half zero was due to the amplifier gain found in the valve assemblies. This performance limitation, however, does not greatly affect the aim of this research. As it will be seen later, the performance requirements of the system need not exceed 2 Hz bandwidth. This requirement causes the limitation to become a moot issue, but if this system was to be used in the future or performance requirements were more demanding, the bandwidth limitation would play a role.

The other technique used in this MIMO analysis is the singular value plot. The singular value plot of a MIMO system is analogous to the Bode plot of a SISO system; both are an expression of the frequency responses of the system. The maximum singular value is the largest gain for any input direction while the minimum singular value of a system is the smallest gain of the system for any input direction. Furthermore, the minimum singular value of the plant, evaluated as a function of frequency, is a useful tool for evaluating the feasibility of achieving acceptable control [2]. It is desirable to have the minimum singular value as large as possible. The singular value of a plant  $G$  is defined as:

$$\sigma(G) = \frac{\|Gu\|_2}{\|u\|_2} \quad (2.3.7)$$

where  $u$  is the input vector. The 2-norm of a vector ( $\|\cdot\|_2$ ) is defined as

$$\|\vec{x}\|_2 = \sqrt{\sum x_i^2}. \quad (2.3.8)$$

From a singular value plot, important information can be gathered. The distance between the maximum and minimum singular value plots gives a good indication of the predictability of a system, as the distance between these plots is essentially the variance

of the gain of the system at a particular frequency. Also, much like a Bode plot, the bandwidth of a MIMO system can be calculated from a singular value plot. A singular value plot of the linear system studied can be seen in Figure 2.3.4

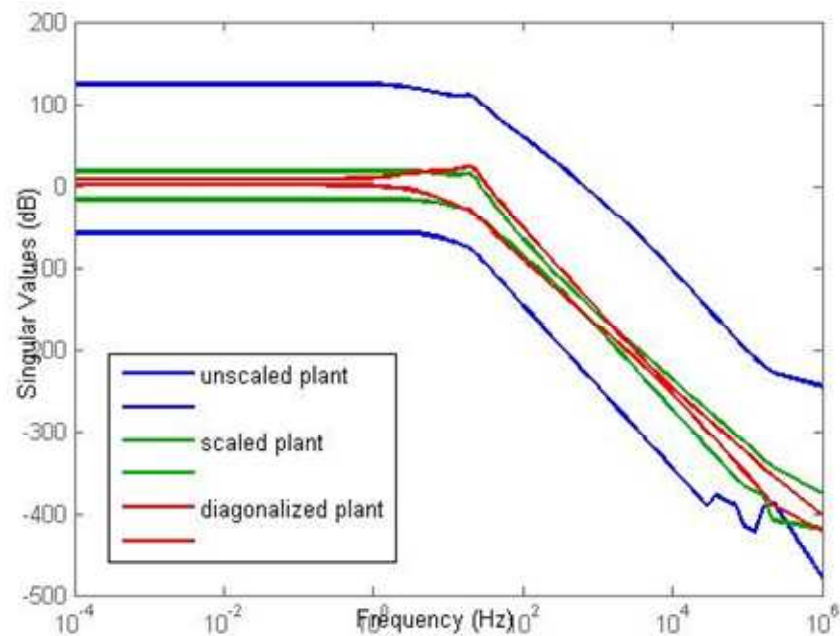


**Fig. 2.3.4 – Singular value plot for the linearized system [8]**

The singular value plots shown in Figure 2.3.4 are for three different systems. The graph denoted as the unscaled plant is just as its name implies: the original model with no input or output scaling. This system is undesirable due to the large difference between the upper and lower singular values at any given frequency. This translates to a highly unpredictable system, for which it would be very difficult to design a controller.

Bringing the maximum and minimum singular values of the system closer together causes the system to behave in a more diagonal manner, meaning it emulates a system which is fully diagonalized or one in which there is no coupling between input and output pairs. To clarify what is meant by coupling, the system is said to be coupled if inputs affect outputs beyond those directly connected in the input output pair. In a two input

two output system, coupling would exist if input one affected output two. The next system analyzed was the scaled plant. This system has been subjected to input and output scaling, which treats every input and output as a percentage of its maximum rather than its true value. As it can be seen, the maximum and minimum singular values of the scaled plant lie much nearer one another, resulting in a more predictable system. The final system analyzed in Figure 2.3.4 is the diagonalized plant. The diagonalization is obtained through multiplying a constant matrix found from the inverse of the DC-gain of the plant transfer function matrix. This system is a modification of the scaled system, with an emphasis placed on decoupling the input-output pairs. From its singular value plot, it can be seen that this system is more predictable than the scaled system, with the exception of a spike at the break frequency of 100 Hz. However, the system is highly coupled and an attempt to completely decouple the system resulted in an oversimplification of the model. The diagonalized model was not used for any future study, due to its inaccuracy when model uncertainty is considered. For the remainder of this analysis, the scaled system was examined.

## **2.4 Categorizing and Modeling System Uncertainty**

An important part of a robustness study is the determination of the variance within the system model. All close-loop control schemes exhibit some level of robustness inherently; however, all control schemes break down when a system varies beyond a point the controller can account for. In this uncertainty study, certain system parameters were allowed to vary and some level of dynamics not fully modeled in the system were accounted for. After a careful study into the uncertain characteristics of a

hydraulic system, it was found that all of the uncertainties within this system could be divided into three categories: valve uncertainty, load uncertainty and fluid (or line) effects. The varying characteristics within each of these categories can be seen in detail with descriptions in Table 2.4.1.

*Table 2.4.1 – Uncertain Characteristics in the IMV hydraulic system*

<i>Valve Uncertainty</i>	
<b>Parameter</b>	<b>Explanation</b>
Valve assembly spring constant	Due to mass manufacturing and sag over time there may be inconsistencies in this value
Solenoid actuation	The force output by the solenoid in the valve assembly may vary over time due to wear
Amplifier gains	As was exhibited in the test data for the IMV, the amplifier displayed non-minimum phase behavior
Spool-centering spring constants	Due to mass manufacturing and sag over time there may be inconsistencies in these values
Spool damping	Wear within the spool will cause damping to decrease over time
Spool leakage	Wear within the spool will cause leakage to increase over time
Manufacturing limitations on springs	Due to finite coil thickness springs cannot always be manufactured at a desired length
Orifice wear	Orifice coefficient can change with wear
Compensator effects	compensator model was assumed ideal when in actuality there are pressure differences on either side of a valve
<i>Load Uncertainty</i>	
<b>Parameter</b>	<b>Explanation</b>
Damping coefficient	Due to cylinder wear, damping coefficients can change
Leakage	Due to cylinder wear, leakage can increase over time
<i>Fluid/Line Effects</i>	
<b>Parameter</b>	<b>Explanation</b>
Fluid Bulk Modulus	Different operating conditions can cause this parameter to vary

Entrained air	Causes a decrease in fluid bulk modulus
Line volume	Stretching of hoses over time or under higher pressures can change this parameter. Also, altering the original design would affect this.
Particles in operating fluid	Will increase line losses and wear

By analyzing the varying characteristics in Table 2.4.1, it was concluded that there was a set of numerical system parameters that, when varied, would encompass the uncertainty of the system within reason. By adjusting these system parameters between their maximum and minimum expected values, the appropriate level of uncertainty in the hydraulic system could be approximated. The uncertainty parameters and their expected ranges for can be found in Table 2.4.2

*Table 2.4.2 – Range of variance for the system’s parameters.*

<b>Parameter</b>	<b>Range</b>
Fluid Bulk Modulus ( $\beta$ )	$\pm 33\%$
Flow Coefficient ( $C_D$ )	0.52 to 0.72 <i>nominally 0.62</i>
Load Force	0 to 1000lbs <i>In addition to the bucket and rod mass</i>
Amplifier gain	$\pm 10\%$
Cylinder Friction	$\pm 25\%$

After defining the uncertain characteristics of the system, an uncertainty model was developed. This analysis was expanded from information found in [8]. An uncertainty model is a transfer function representing an error in the output of the system. The



uncertainty model used in this research is multiplicative output uncertainty which can be seen in Figure 2.4.1 as  $w_o$ .

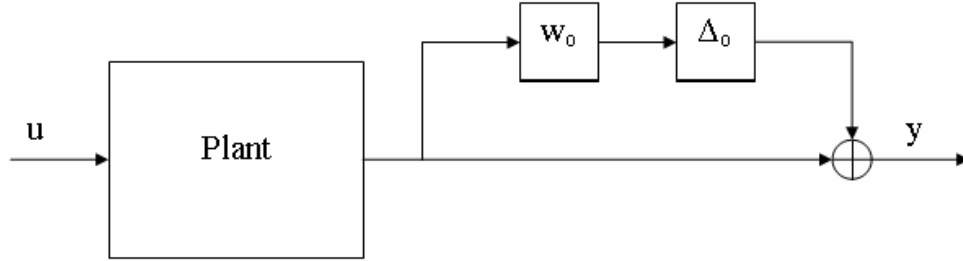


**Fig. 2.4.1 – Output multiplicative uncertainty**

The accompanying term  $\Delta_o$  is the set of all transfer functions whose maximum singular value is less than one. The  $\Delta_o$  term is a scaling factor; essentially a gain within the system that will amplify its input to between  $\pm 100\%$  ( $\pm 1$ ). This term is, in practical usage, not considered in quantitative calculations and is generally only addressed in mathematical derivations of the robust control analysis. The focus of this project will remain on the output uncertainty  $w_o$ .

To obtain an uncertainty description, the set of all possible plant perturbations were examined. By changing each parameter in Table 2.4.2 individually and linearizing the system again for each configuration, a series of perturbed plants were created. The plant perturbations were created using:

$$\left[ (G_p - G_{nom}) G_{nom}^{-1} \right] \quad (2.4.1)$$

This set of perturbed plants,  $G_p$ , was then used to construct the uncertainty description:

$$w_o = \max \bar{\sigma} \left[ (G_p - G_{nom}) G_{nom}^{-1} \right] \quad (2.4.2)$$

over all perturbed plant models  $G_p$ . The output uncertainty of the system is a transfer function fit of the highest maximum singular value plot among all plant variations. This result is shown graphically in Figure 2.4.2.

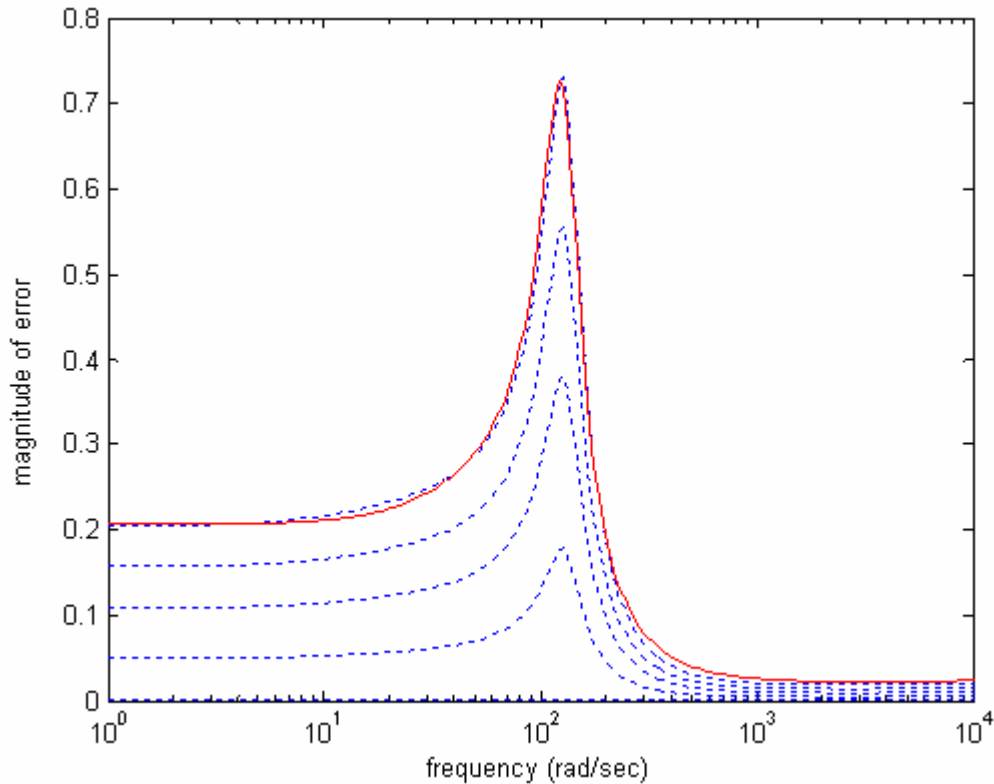


**Fig 2.4.2 – Output uncertainty transfer function**

In Figure 2.4.2, many plant perturbations can be seen as dashed lines. The darkened line is the transfer function,  $w_o$ , created to bound all possible perturbations; it is the worst possible variation the system could undergo. It can be seen that the plant will vary by approximately 20% at low frequency and around 5% at high frequency. At 100Hz the largest plant variation exists. The plant varies by approximately 75% at this frequency. The transfer function,  $w_o$ , will be used for nominal and robustness analysis in Chapter 6.

## Chapter 3

### $H_\infty$ CONTROL MECHANISMS

#### 3.1 Necessity of $H_\infty$ Control Routines

LQG or linear quadratic Gaussian control routines, based on optimal filtering work of Wiener in the 1940s, were utilized in the 1960s as a way to accurately control space vehicles and minimize fuel consumption. Though these techniques are used successfully by aerospace engineers, LQG is difficult to apply reliably to many industrial problems due to the reliance on highly accurate system models and the assumption of white noise disturbances [2]. These deficiencies cause LQG control to often lack robustness characteristics that are appropriate for many applications. This characterization of low robustness was brought to the attention of the controls community in 1978 by Doyle. In the 1980s, researchers such as Zames, Helton, Glover and Doyle developed  $H_2$  and  $H_\infty$  methods to answer specific robustness concerns of LQG. This is not to say that LQG cannot show robust characteristics or that it is not applied successfully in industry. The desire was to create new control systems that showed robustness characteristics that were superior to LQG.

#### 3.2 The $H_\infty$ Control Problem

For the sake of discussion in this research,  $H_\infty$  methods alone will be of interest. This narrowed view is justified by the recognition that  $H_2$  and  $H_\infty$  methodologies are similar in that: both require the solutions to two Riccati equations, both give controllers

of state-dimension equal to the generalized plant, P, and both show separation structure in their controllers that are already seen in LQG control [2]. It is important to note, however, that  $H_\infty$  controllers provide a sub-optimal controller which differs from  $H_2$  control which provides optimal and unique controllers. It should be noted that (s) is often dropped as a convention.

The general problem formulation of  $H_\infty$  problems are described by

$$\begin{bmatrix} z \\ v \end{bmatrix} = P(s) \begin{bmatrix} w \\ u \end{bmatrix} = \begin{bmatrix} P_{11}(s) & P_{12}(s) \\ P_{21}(s) & P_{22}(s) \end{bmatrix} \begin{bmatrix} w \\ u \end{bmatrix} \quad (3.2.1)$$

$$u = K(s)v \quad (3.2.2)$$

with a generalized plant P given by

$$P = \begin{bmatrix} A & B_1 & B_2 \\ C_1 & D_{11} & D_{12} \\ C_2 & D_{21} & D_{22} \end{bmatrix}. \quad (3.2.3)$$

The variables are:  $u$ , the control variables,  $v$ , the measured variables,  $w$ , the exogenous signals such as disturbances and  $z$ , the error signal to be minimized. The generalized plant model schematic can be seen in Figure 3.2.1.

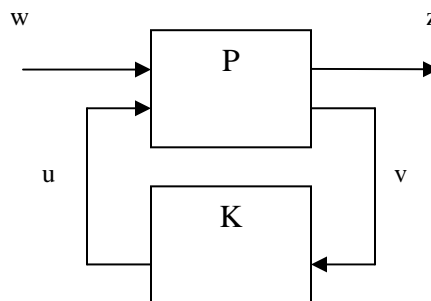


**Fig 3.2.1 – The Generalized plant model**

By referring to Skogestad and Postlethwaite [2], it can be seen that the closed-loop transfer function from  $w$  to  $z$  can be given via the linear fractional transformation

$$z = F_l(P, K)w \quad (3.2.4)$$

where

$$F_l(P, K) = P_{11} + P_{12}K(I - P_{22}K)^{-1}P_{21}. \quad (3.2.5)$$

Using the linear fractional transformation, the  $H_\infty$  control problem is to find a controller,  $K$ , that minimizes

$$\|F_l(P, K)\|_\infty = \max_{\omega} \bar{\sigma}(F_l(P, K)(j\omega)). \quad (3.2.6)$$

The  $\infty$ -norm can be thought of as the ratio of input to output vector 2-norms.

$$\|F_l(P, K)\|_\infty = \max_{\omega(t) \neq 0} \frac{\|z(t)\|_2}{\|w(t)\|_2} \quad (3.2.7)$$

where

$$\|z(t)\|_2 = \sqrt{\int_0^\infty \sum |z_i(t)|^2 dt} \quad (3.2.8)$$

Because the controller does not require optimal solutions, or that optimal solutions are too difficult to calculate, the value  $\gamma_{\min}$  is defined. The problem then becomes to find a controller,  $K$ , such that

$$\|F_l(P, K)\|_\infty < \gamma \quad (3.2.9)$$

where  $\gamma > \gamma_{\min}$ . This process is then done iteratively so that the controller approaches an optimal solution. Design of  $H_\infty$  controllers involves shaping the maximum singular value of specified transfer functions over specific frequencies. These design trade-offs have been identified earlier in this document.

### 3.3 Mixed Sensitivity $H_\infty$ Control

Mixed sensitivity (MS) control is a routine named as such due to the transfer function shaping methods used. The MS control routine aims to find a controller that gives the desired closed-loop sensitivity transfer functions  $S$ ,  $T$  and  $KS$ .  $S$  is defined as the sensitivity function which is derived mathematically from:

$$S = (I + GK)^{-1} \quad (3.3.1)$$

$T$  is defined as the closed-loop transfer function which is derived mathematically from:

$$T = (I + GK)^{-1} GK \quad (3.3.2)$$

These quantities come from the classic one degree-of-freedom feedback configuration shown in Figure 3.3.1.

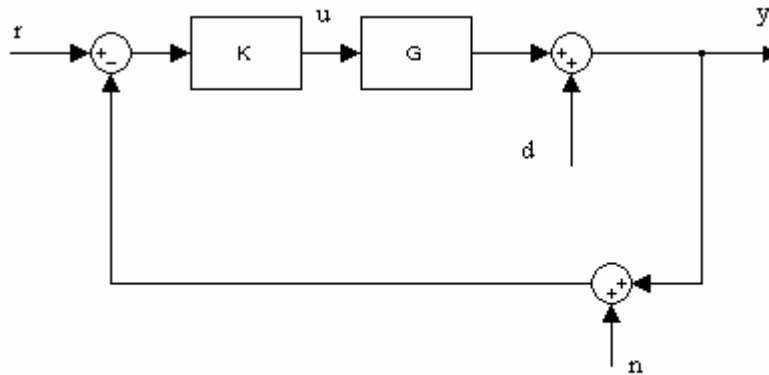


**Fig. 3.3.1 – One degree-of-freedom feedback configuration**

From Figure 3.3.1, two important relationships can be seen:

$$y(s) = T(s)r(s) + S(s)d(s) - T(s)n(s) \quad (3.3.3)$$

$$u(s) = K(s)S(s)[r(s) - n(s) - d(s)] \quad (3.3.4)$$

These relationships determine several closed-loop objectives, in addition to the requirement that  $K$  stabilizes  $G$ : 1) to reject disturbances to the system, the maximum

singular value of  $S$  must be small, 2) to reject noise, the maximum singular value of  $T$  must be small, 3) for reference tracking, the minimum and maximum singular value of  $T$  should be approximately 1, 4) for control energy reduction make the maximum singular value of  $KS$  small, 5) for robust stability when there are additional perturbations, make the maximum singular value of  $KS$  small and 6) for robust stability when there is multiplicative output perturbation, make the maximum singular value of  $T$  small [2]. From these performance goals, it can be seen that there exists a great deal of trade-off between competing objectives. Balancing  $S$  and  $T$  weighting is tricky but it is easily seen that making  $KS$  small is advantageous.

The general design goal is to minimize:

$$\left\| \begin{array}{l} S \ w_P \\ T \ w_T \\ KS \ w_U \end{array} \right\|_{\infty} \quad (3.3.5)$$

where  $w_P$  is the weight associated with the error due to reference input,  $w_T$  is the weight associated with the effect of noise and  $w_U$  is the weight associated with the control effort of the system. In the event of nonminimum phase, which is the case in this system, the stability requirement will limit the bandwidth achievable by adjusting controller gains, so it is useful to minimize  $S$  and  $KS$ . This system can be represented by the following block diagram

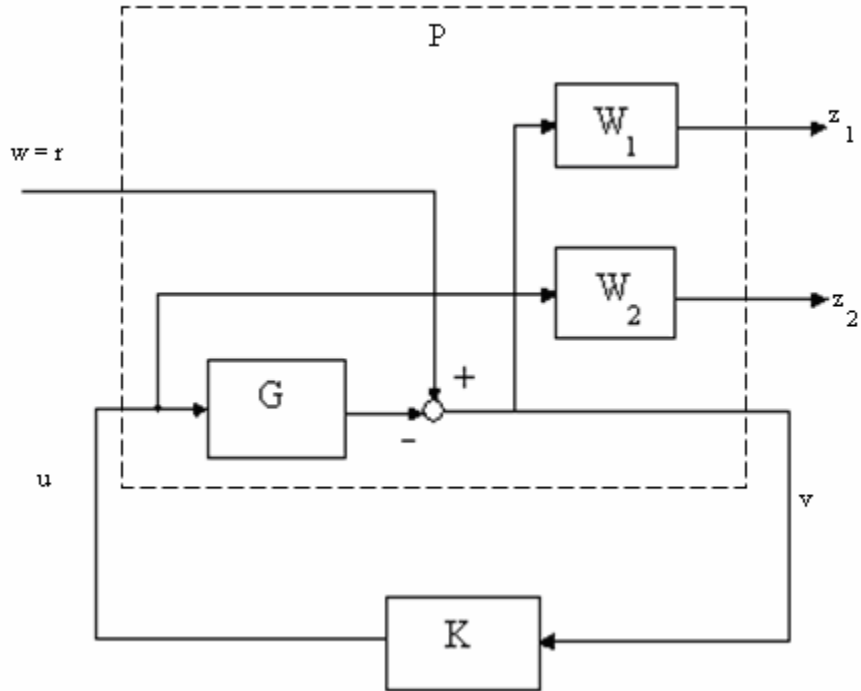


**Fig 3.3.2 – S/KS form of MS for tracking**

In Figure 3.3.2,  $W_1$  and  $W_2$  are  $w_P$  and  $w_U$  respectively.  $P$  is defined as

$$P = \begin{bmatrix} w_P & -w_P G \\ 0 & w_U \\ I & -G \end{bmatrix}. \quad (3.3.6)$$

It is important to note that all weights,  $w_i$ , should be stable [2]. The optimization routine *hinfsyn.m* [9] is used for this design.

### 3.4 MacFarlane-Glover $H_\infty$ Loop-shaping

Combining classical loop-shaping techniques and robust stabilization, this technique was created by MacFarlane and Glover in the 1989 [2]. This technique is a two step process: 1) The open-loop plant is augmented with pre and post-compensators to shape the singular values of the frequency response and 2) the resulting plant is stabilized



with respect to coprime factor uncertainty using  $H_\infty$  optimization. This technique also does not require  $\gamma$ -iteration for its solution. The shaped plant in need of improved robustness for this research was a compensator which was simply a PID controller tuned for performance with little regard to stability. The stabilizing controller created by MacFarlane and Glover (MG) uses a normalized left coprime factorization of the plant and standard robust stabilization transforms. The details of that process can be found in Skogestad and Postlethwaite's text [2]. MacFarlane and Glover found that the lowest value of  $\gamma$  and the corresponding maximum stability margin  $\varepsilon$  is described as:

$$\gamma_{\min} = \varepsilon_{\max}^{-1} = \left\{ 1 - \left\| \begin{bmatrix} N & M \end{bmatrix} \right\|_H^2 \right\}^{-\frac{1}{2}} = (1 + \rho(XZ))^{\frac{1}{2}} \quad (3.4.1)$$

where  $N$  and  $M$  are from the coprime factorization of  $G$ ,  $\|\cdot\|_H$  is the Hankel norm and  $\rho$  is the maximum eigenvalue.  $X$  and  $Z$  are the solutions to the following algebraic Riccati equations for the state-space realization  $(A,B,C,D)$  of  $G$ :

$$(A - BS^{-1}D^T C)Z + Z(A - BS^{-1}D^T C)^T - ZC^T R^{-1} CZ + BS^{-1}B^T = 0 \quad (3.4.2)$$

where

$$R = T + DD^T \quad (3.4.3)$$

$$S = I + D^T D \quad (3.4.4)$$

and

$$(A - BS^{-1}D^T C)X + X(A - BS^{-1}D^T C)^T - XBS^{-1}B^T X + C^T R^{-1} C = 0. \quad (3.4.5)$$

The stabilizing controller is given by

$$K \overset{\Delta}{=} \begin{bmatrix} A + BF + \gamma^2 (L^T)^{-1} ZC^T (C + DF) & \gamma^2 (L^T)^{-1} ZC^T \\ B^T X & -D^T \end{bmatrix} \quad (3.4.5)$$

where

$$F = -S^{-1}(D^T C + B^T X) \quad (3.4.6)$$

$$L = (1 - \gamma^2)I + XZ. \quad (3.4.7)$$

This control ensures that for a specified  $\gamma > \gamma_{\min}$

$$\left\| \begin{bmatrix} K \\ I \end{bmatrix} (I - GK)^{-1} M^{-1} \right\|_{\infty} \leq \gamma \quad (3.4.8)$$

which is the stability criterion derived in Skogestad and Postlethwaite. To solve this, there is a Matlab command from Skogestad and Postlethwaite, *coprimeunc.m* [10] that was utilized. Its inputs are the state-space realization of the shaped-plant and a  $\gamma_{\text{rel}}$  term that is typically 1.1. The actual  $\gamma$  used in [10] is  $\gamma_{\text{rel}} * \gamma_{\min}$  which is done internally in the program. The function outputs the state-space realization of the stabilizing controller,  $K$ .

### 3.5 Two Degrees-of-freedom $H_{\infty}$ Control

Many control design problems have two-degrees of freedom available for design, most reduce to using a single-degree error signal for design. At times, this is not sufficient for appropriate tracking. MacFarlane-Glover  $H_{\infty}$  Loop-shaping allows for sufficient tracking characteristics with the use of a constant prefilter to ensure proper steady-state tracking. However, work in the early 1990s lead by Hoyle and Limebeer was done to augment MacFarlane and Glover's control design to be a true two-degree of freedom system [2]. This control routine allows for the feedback part of the controller to be designed to meet robust stability and reject system disturbances similar to a single-degree of freedom system while the reference input portion of the controller matches performance requirements established via reference input shaping. A prefilter gain is used

to enforce accurate closed-loop response matching to the reference input model. A model of the control system can be seen in Figure 3.5.1

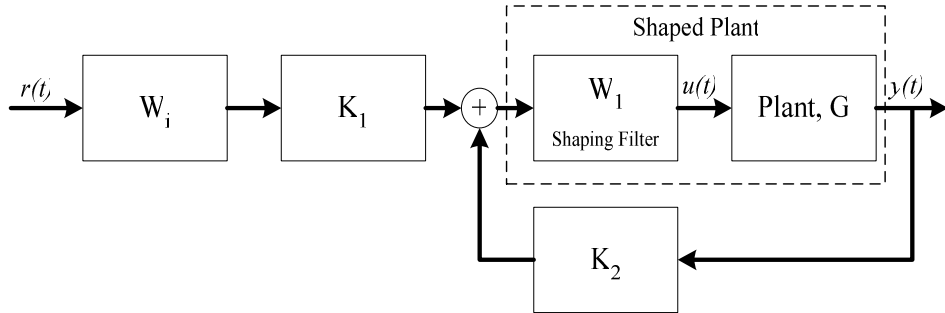


**Fig 3.5.1 – Two degrees-of-freedom design schematic**

The design problem is to find a stabilizing controller  $K = [K_1 \ K_2]$  for the shaped-plant,  $G_s$ , that minimizes the  $H_\infty$  norm of the transfer function between input and output signals via coprime factorization similar to the method in section 3.4. The general equation is solved sub optimally via  $\gamma$ -iteration. The control signal to the shaped plant is defined as:

$$u_s = [K_1 \ K_2] \begin{bmatrix} \beta \\ y \end{bmatrix} \quad (3.5.1)$$

where  $K_1$  is the prefilter,  $K_2$  is the feedback controller,  $\beta$  is the scaled reference and  $y$  is the measured output. The purpose of the prefilter is to adjust low frequency gains and ensure that

$$\left\| (I - G_s K_2)^{-1} G_s K_1 - T_{ref} \right\|_\infty \leq \gamma \rho^{-2} \quad (3.5.2)$$

where  $T_{ref}$  is the desired closed-loop transfer function designed to meet time-domain based design requirements and  $\rho$  is a scalar parameter that can be increased to put more emphasis on model matching during the optimization as a trade off to robustness. To define a generalized plant  $P$ , the shaped-plant and closed-loop transfer function are defined as a state-space realization:

$$G_s = {}^s \begin{bmatrix} A_s & B_s \\ C_s & D_s \end{bmatrix} \quad (3.5.3)$$

$$T_{ref} = {}^s \begin{bmatrix} A_r & B_r \\ C_r & D_r \end{bmatrix} \quad (3.5.4)$$

The shaped-plant is defined as the plant gained by the compensator. The generalized plant then follows as:

$$P = \begin{bmatrix} A_s & 0 & 0 & (B_s D_s^T + Z_s C_s^T) R_s^{-1/2} & B_s \\ 0 & A_r & B_r & 0 & 0 \\ 0 & 0 & 0 & 0 & I \\ C_s & 0 & 0 & R_s^{1/2} & D_s \\ \rho C_s & -\rho^2 C_r & -\rho^2 D_r & \rho R_s^{1/2} & \rho D_s \\ 0 & 0 & \rho I & 0 & 0 \\ C_s & 0 & 0 & R_s^{1/2} & D_s \end{bmatrix} \quad (3.5.5)$$

where  $R_s = I + D_s D_s^T$  and  $Z_s$  is defined via Eq. (3.4.2). The algorithm for solving this controller can be seen in Skogestad and Postlethwaite's *hinf2dof.m* [11]. One further prefilter,  $W_i$  is needed to ensure steady-state error matching which is not guaranteed after undergoing optimization which solely aims to minimize the  $\infty$ -norm.

$$W_i \stackrel{\Delta}{=} [W_o (I - G_s(0)K_2(0))^{-1} G_s(0)K_1(0)]^{-1} T_{ref}(0) \quad (3.5.6)$$

where  $W_o$ , the output selection matrix, is typically equal to the identity matrix. The output selection matrix allows the designer to select specific outputs that are required for control.

## Chapter 4

### APPLICATION OF CONTROL ROUTINES

#### 4.1 Performance Requirements

A goal of any control system is to satisfy requirements of performance. The most common among these are a desired bandwidth  $\omega_B$ , an allowable steady-state error  $A$ , and an allowable high-frequency error  $M$ . These three criteria can be assembled into the performance weighting transfer function  $w_p$  by using:

$$w_{Pi} = \frac{s/M_i + \omega_{Bi}}{s + \omega_{Bi}A_i} \quad (4.1.1)$$

for each  $i$ -th output. The two outputs considered are the load velocity error and the pressure drop error across the main pump-to-cylinder head-end valve. The specific values associated with each of the performance weights can be seen in Table 4.1.1.

*Table 4.1.1 Performance requirements for velocity and margin pressure control.*

Criteria	Velocity Output	Margin Pressure Output
<b>Bandwidth</b>	1.5 Hz	1 Hz
<b>Steady-state Error</b>	5%	15%
<b>High Frequency Error</b>	200%	200%

The design requirements listed are tested in the frequency domain robustness analysis to verify that the controller will satisfy all criteria for all possible plant perturbations. These requirements will be explored in detail in Chapter 6.

## 4.2 Baseline PID Design

The PID controller was first designed. This design was done for two reasons: 1) to create a baseline for comparison and 2) the MacFarlane-Glover and Two Degree-of-freedom controller is designed to utilize an existing performance controller already in place. Because the modern controllers to be used were created to add stability and robustness to the system, the baseline PID controller was designed with performance requirements solely in mind. Due to PID being a SISO design technique and the system being a MIMO system, two PID controllers were designed, one for each controlled output. The PID configuration used is defined as:

$$K(s) = K_p + \frac{K_I}{s} + \frac{K_D s}{s/p + 1} \quad (4.2.1)$$

This form of the PID has an approximated derivative term. This form is used due to numerical issues in Matlab that prevent a traditional PID form from being used and  $p$  is a fast pole. The two PID controllers used are as follows:

$$PID_{MP} = \frac{0.8s + 251.3}{s + 268.3} \quad (4.2.2)$$

$$PID_V = \frac{0.1s^2 + 68.83s + 3142}{s^2 + 628.3s} \quad (4.2.3)$$

The design methodology was to tune the P component to the point of instability and then tune the I and D component until steady-state response and dynamic response were appropriate. The controller was tested on the linearized plant model; the results of those simulations can be seen in Figures 4.2.1 and 4.2.2.

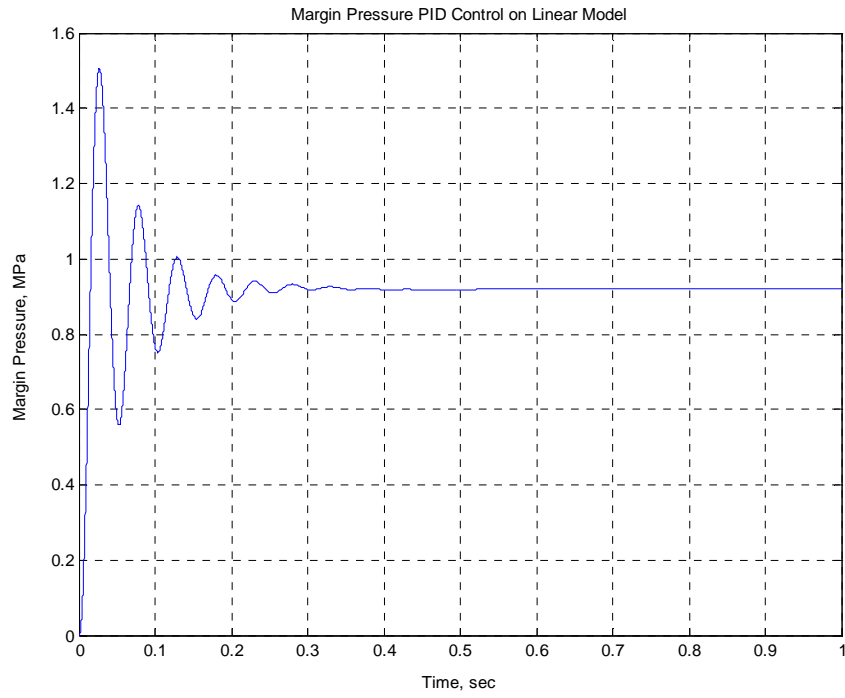


**Fig. 4.2.1 – Margin pressure step response for linear PID**

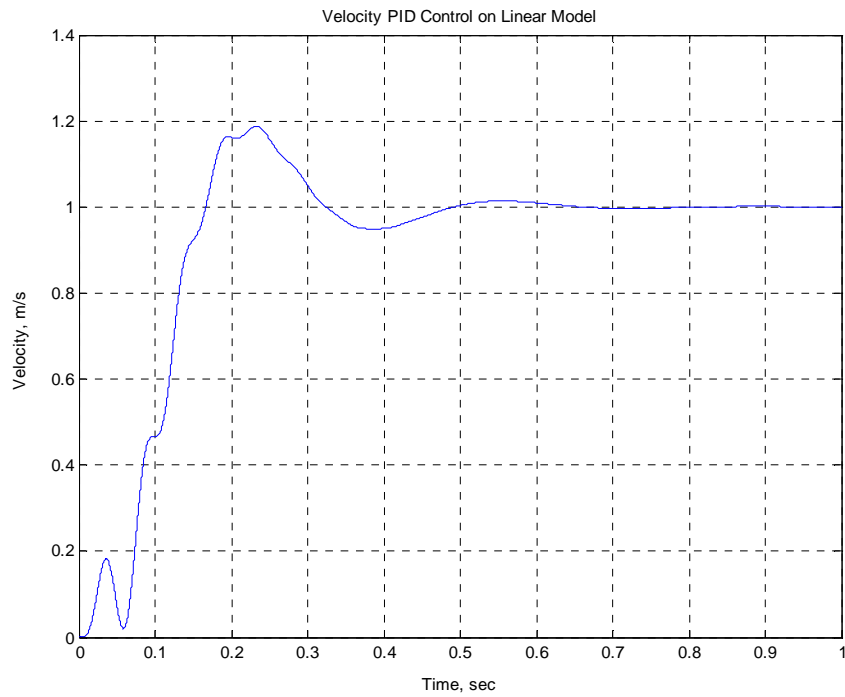


**Fig. 4.2.2 – Velocity step response for linear PID**

In Figure 4.2.1, the margin pressure shows very quick rise time with an overshoot of approximately 50%. The steady-state error of the response is approximately 10% which is within the 15% acceptable from performance requirements. The velocity response in Figure 4.2.2 shows slower rise time but a less pronounced overshoot and also exhibits zero steady-state error. The controllers were then tested on the nonlinear model. The margin pressure has a commanded input of 1 MPa through a step input; the velocity input follows a square-wave input that varies between 0.25 and 0.45 m/s commanded input. The nonlinear control responses can be seen in Figures 4.2.3 and 4.2.4.

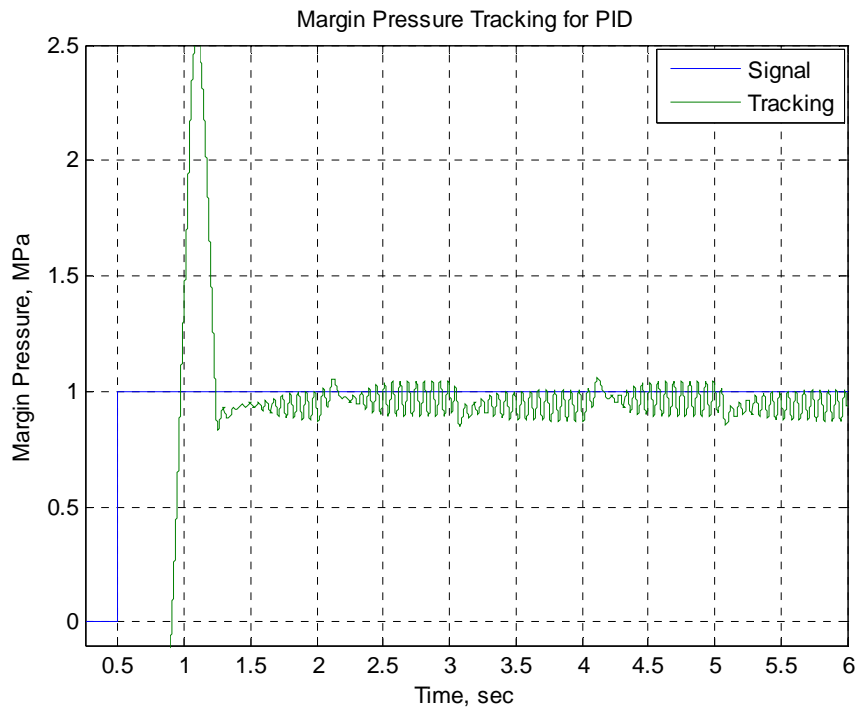


**Fig 4.2.3 – Margin pressure response for PID control on the nonlinear model**



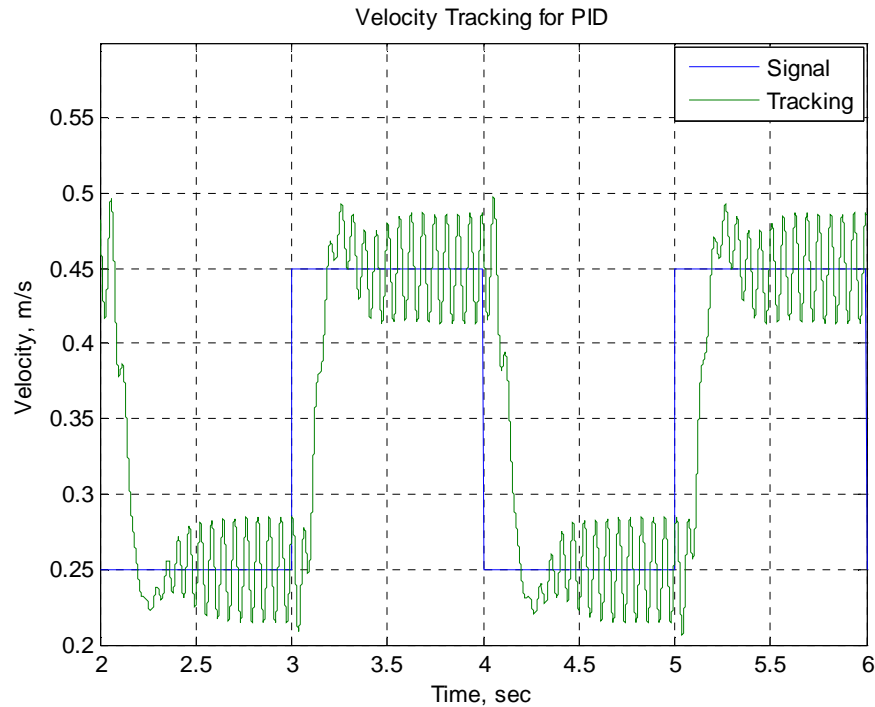


**Fig. 4.2.4 – Velocity response for PID control on the nonlinear model**

In Figure 4.2.3, it can be seen that there exists a certain amount of coupling between the margin pressure and velocity control. This is evident from the periodic fluctuation in pressure roughly every second. Both of these control performances show a certain amount of tendency toward instability as seen by the quick oscillations in the performance plots. Steady-state values are comparable to the linear responses. It is hard to comment on whether or not the margin pressure response is as fast as it was in the linear model due to the pre-step margin pressure fluctuation in the nonlinear model. However, it can be commented that the velocity response is very similar to the linearized response with respect to time. The velocity response does show an increase in high frequency oscillations that were not present in the linear model.

### 4.3 Mixed Sensitivity Design - Application

For mixed sensitivity design, the methodology outlined in Chapter 3.3 was used. In that section, the terms  $S$  and  $SK$  were identified as important design aspects for this system. This reduces the quantities to minimize in design as:

$$\left\| \begin{array}{c} Sw_p \\ SKw_u \end{array} \right\|_{\infty} \quad (4.3.1)$$

To apply this control to a MIMO system, a matrix of weights was chosen for each input. The performance weight,  $w_p$ , uses Eq. 4.1.1 as its basis. For margin pressure performance weighting,  $A=0.1$ ,  $\omega_B=0.001$  Hz and  $M=10$ . For velocity performance weighting,  $A=0.05$ ,  $\omega_B=0.8$  Hz and  $M=2$ . The control effort weight,  $w_u$ , was set to  $1/100$ . These design values are the final control values after iteration during the design process. The controller,  $K$ , was determined via optimization using the weighting matrices and  $P$ , as defined in Eq. 3.3.2. One drawback of mixed sensitivity control is that the controller,  $K$ , is high order. To reduce the model, techniques outlined in Skogestad and Postlethwaite were used. The linear responses to step inputs can be seen in Figures 4.3.1 and 4.3.2.

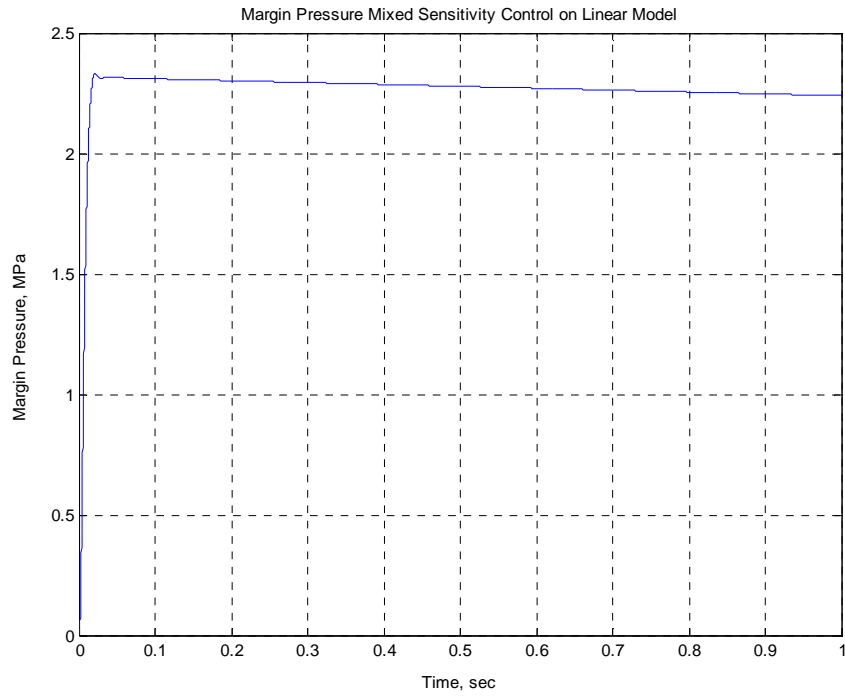


**Fig. 4.3.1 – Margin pressure step response for linear mixed sensitivity**

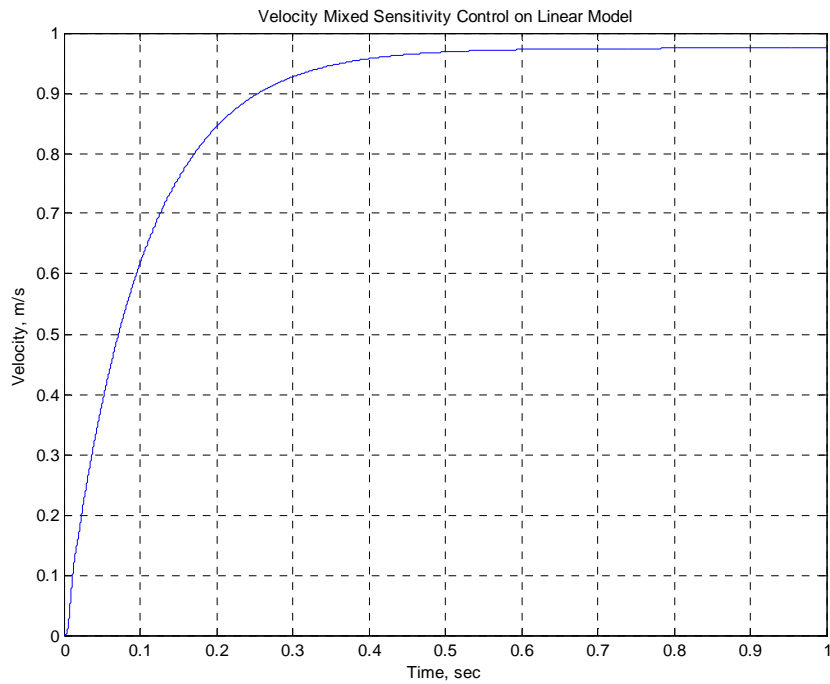


**Fig. 4.3.2 – Velocity step response for linear mixed sensitivity**

From Figure 4.3.1, it can be seen that the response time for margin pressure is extremely fast and that the overshoot and settling time is very large. The velocity response in Figure 4.3.2 shows a much better response. It exhibits a slow rise time but lacks overshoot and settling time issues that are present in the margin pressure response. Also, the steady-state error is within acceptable bounds. The iterative process used to create these weights was done via examination of nonlinear response. It was found that the inputs and output pairs were highly coupled, and that the only way to get proper response in velocity was to quicken the response in margin pressure. This is what leads to such an atypical response in the margin pressure response. The nonlinear responses can be seen in Figures 4.3.3 and 4.3.4.

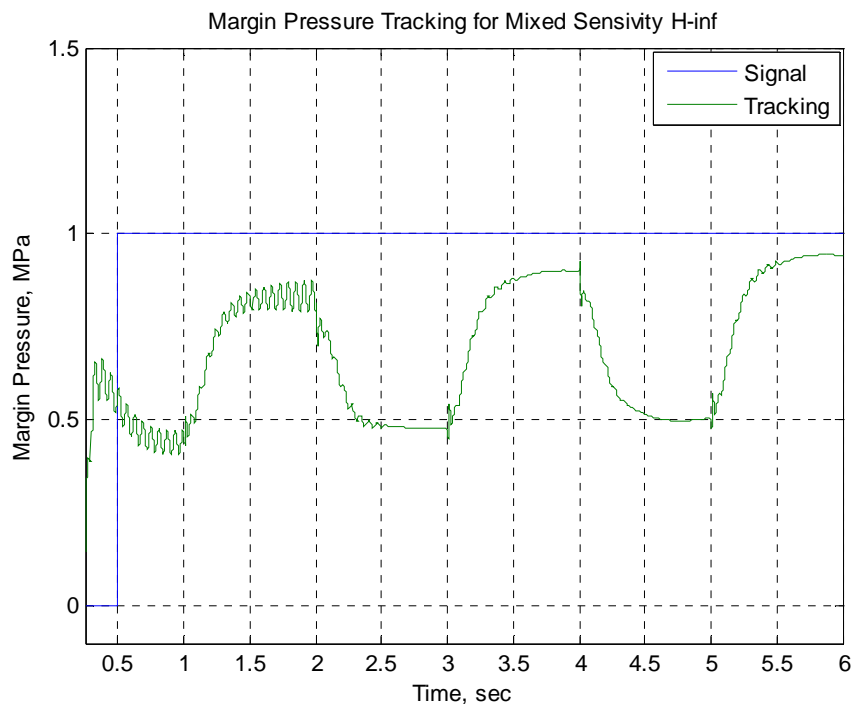


**Fig. 4.3.3 – Margin pressure response for mixed sensitivity control on the nonlinear model**

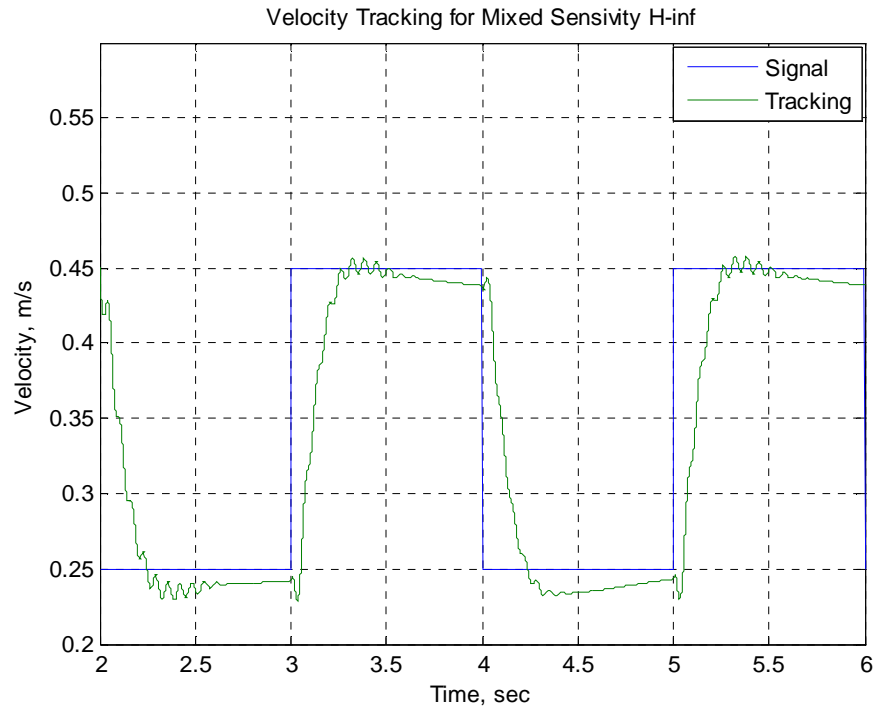


**Fig. 4.3.4 – Velocity response for mixed sensitivity control on the nonlinear model**

Several interesting aspect of the system can be seen from the application of this controller. In Figure 4.3.3, the strong coupling between input and output pairs can be seen. The margin pressure response follows the linear behavior of slowly approaching the correct steady-state behavior over time, but also shows response to the square wave signal being commanded for the velocity. The velocity response in Figure 4.3.4 shows acceptable rise time and steady-state is within the acceptable bounds.

#### **4.4 MacFarlane-Glover $H_\infty$ Loop-shaping – Application**

MacFarlane-Glover (MG)  $H_\infty$  loop shaping utilizes a PID design for performance and creates a controller that improves robustness. This controller bridges the gap between SISO PID design and MIMO  $H_\infty$  robust control design. To design the MG controller, the initial PID controller was used and the robustness controller was created

using optimization techniques. To tune the system, modifications to the PID can be made but with emphasis remaining on performance rather than stability. However, because one research goal was to add robustness to a system without designing a new controller, modifying the PID was not appropriate. The only design variable that remained was tuning  $\gamma_{rel}$  which severely limited the flexibility of this design. The system control model is as follows:

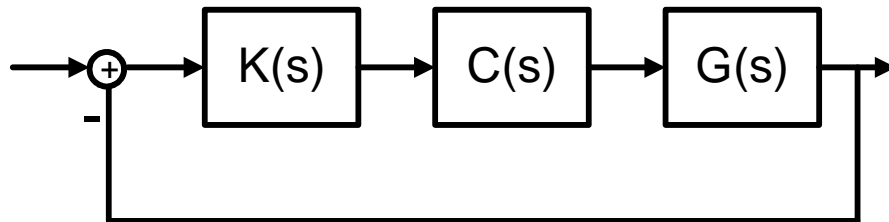


**Fig 4.4.1 – Control schematic for MacFarlane-Glover control**

In Figure 4.4.1,  $K(s)$  is the stabilizing controller and  $C(s)$  is the PID controller governing performance. Implementation suffers from the same problem as the MS control design: high order system with fast poles. This problem is alleviated with model order reduction. The linear responses for margin pressure and velocity can be seen in Figures 4.4.2 and 4.4.3 respectively.

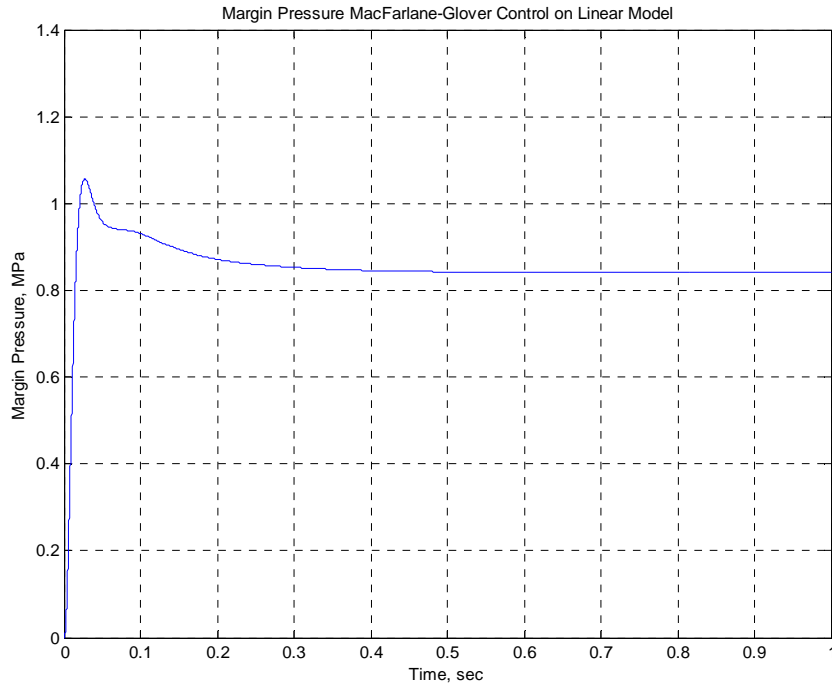


**Fig. 4.4.2 – Margin pressure step response for linear MacFarlane-Glover**

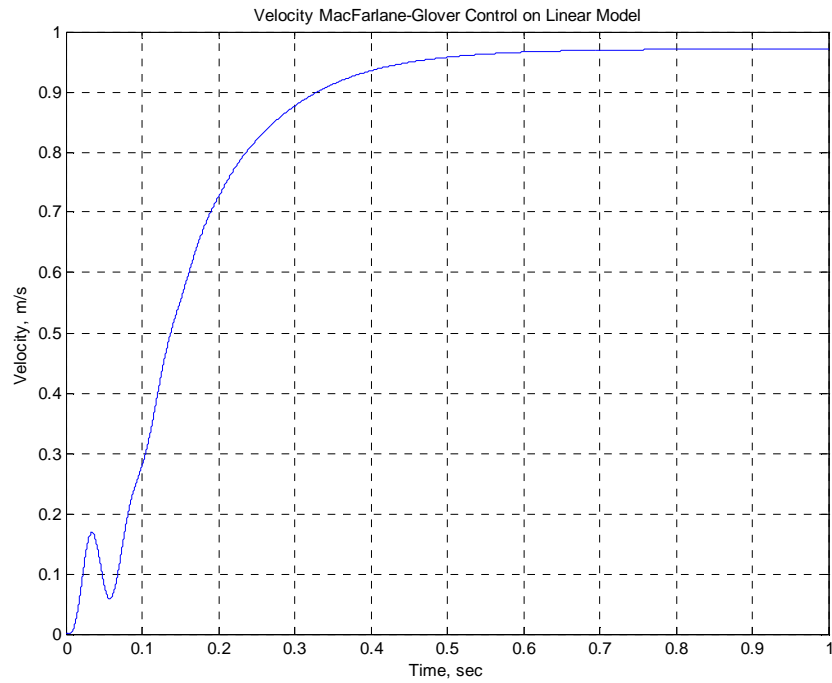


**Fig. 4.4.3 – Velocity step response for linear MacFarlane-Glover**

The margin pressure response in Figure 4.4.2 shows once again very quick rise time characteristics as well as quick settling times. The steady-state error associated with the response is large and exceeds the 15% design requirement. The velocity response in Figure 4.4.3 shows a slower rise time than the PID but does show increased damping as evident by the reduction in overshoot. It should be noted that both linear responses exhibit increased stability in the form of increased damping that reduces oscillations in the response seen in the PID controller. The responses for the nonlinear model can be seen in Figures 4.4.4 and 4.4.5.

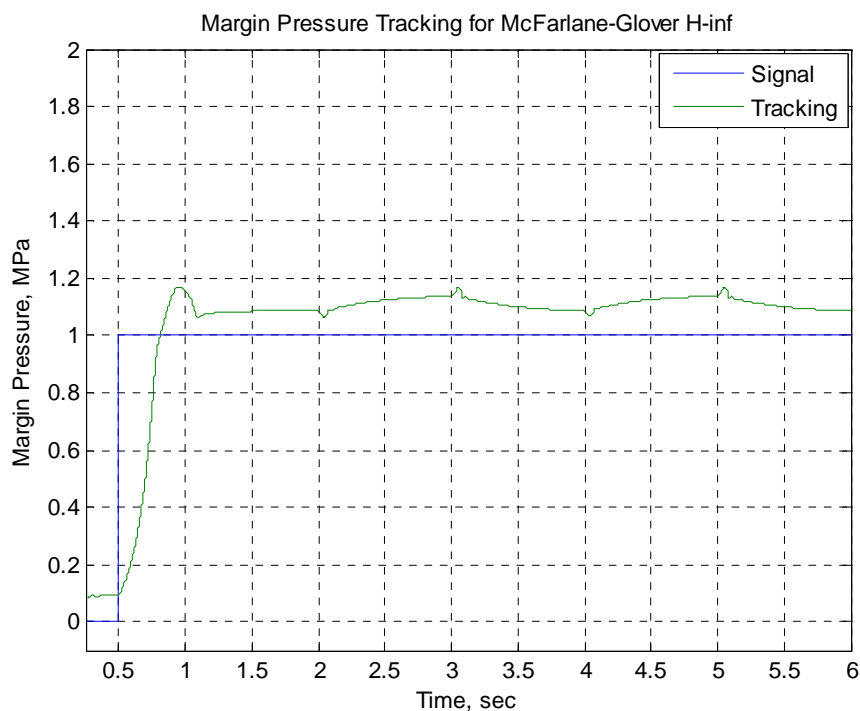


**Fig. 4.4.4 – Margin pressure response for MacFarlane-Glover control on the nonlinear model**



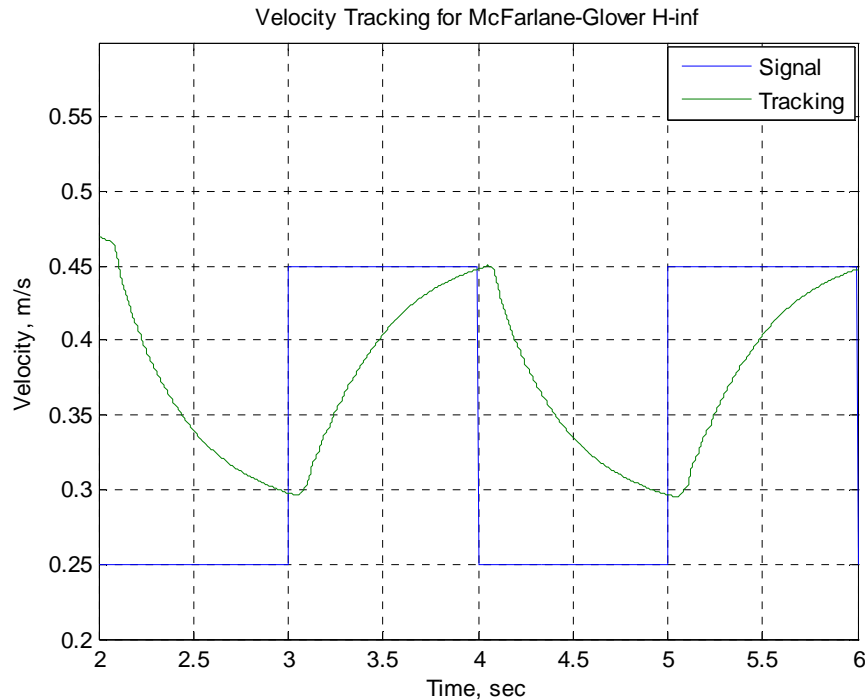


**Fig. 4.4.5 – Velocity response for MacFarlane-Glover control on the nonlinear model**

From Figure 4.4.4, the margin pressure response exhibits quick rise time and quick settling time and also shows steady-state results that are within the acceptable 15% range. Furthermore, the margin pressure result shows that the control routine did achieve a certain level of decoupling. The margin pressure response is not heavily affected by the square wave commanded velocity. In Figure 4.4.5, however, the velocity response did not reach satisfactory results. The velocity response shows very slow response to the commanded inputs causing the system to never reach the minimum commanded velocity. This results in very poor tracking and poor steady-state response.

#### 4.5 Two Degrees-of-freedom $H_\infty$ Control – Application

The two degrees-of-freedom controller has one primary difference in its control design: instead of controlling a single error signal, this controller routine utilizes both measured state signals and reference input signals separately. This allows the designer to prescribe performance characteristics for the desired tracking response. This controller uses the PID controller designed for performance and input reference characteristics to define the desired closed-loop response; an optimal controller algorithm is used to find a controller for the input criteria and creates a controller that adds robustness to the system. The scheme used for the system can be seen in Figure 3.5.1.

The desired closed-loop transfer function,  $T_{ref}$ , is defined as:

$$T_{ref}(s) = \frac{\omega_n^2}{s^2 + 2\zeta\omega_n s + \omega_n^2} \quad (4.5.1)$$

A matrix of desired closed-loop transfer functions is made with the diagonal terms being the transfer function associated with each output, while the off diagonals are zero.

Having zeros in the off diagonal terms help ensure that coupling between input/output pairs does not occur. For margin pressure, the desired natural frequency is 2.1 Hz and the desired damping ratio is 0.7. For velocity, the desired natural frequency is 1.7 Hz and the desired damping ratio is 0.7. The damping ratios for both represent a 5% overshoot. The value of natural frequency was found iteratively by trial and error in tuning the performance of the controller. It should be noted that natural frequency was solely modified due to bandwidth limitations driving the control deficiencies. The response of the desired closed-loop matrix,  $T_{ref}$ , can be seen in Figure 4.5.1.

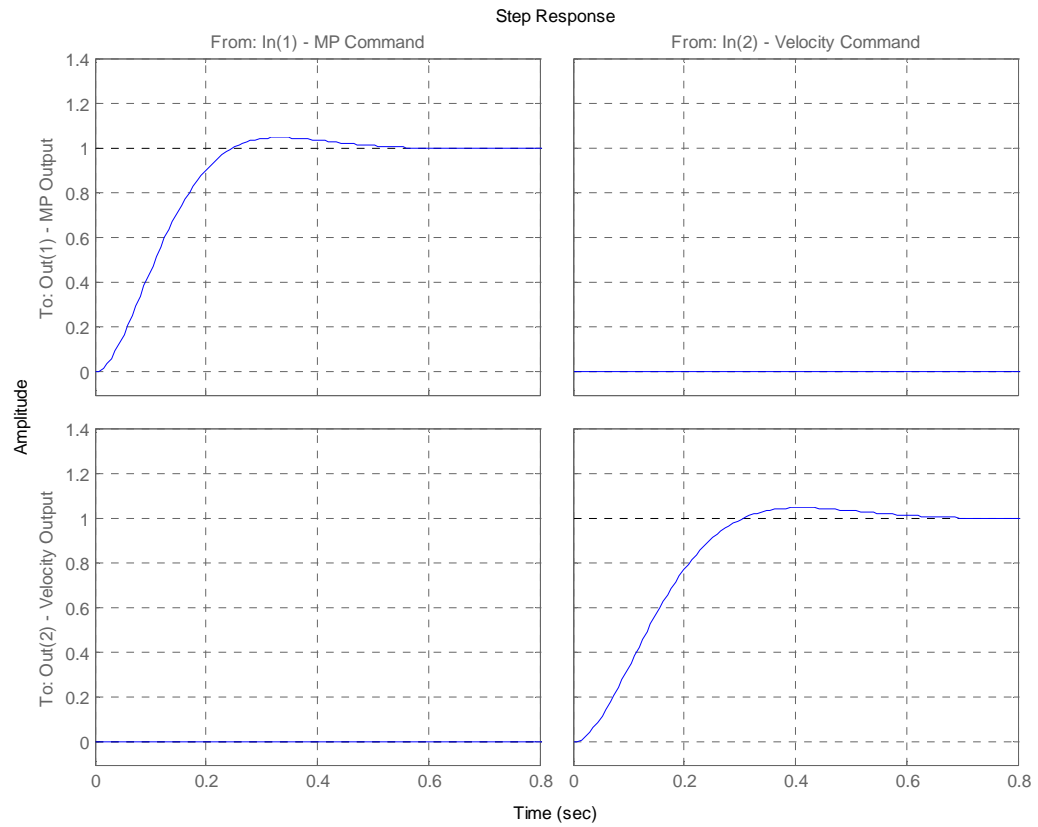


**Fig. 4.5.1 – Step response of the desired closed-loop transfer function matrix**

In Figure 4.5.1, both responses exhibit no steady-state error, minimal overshoot and fairly quick rise and settling times. The linear simulations of the control routine can be seen in Figures 4.5.2 and 4.5.3.

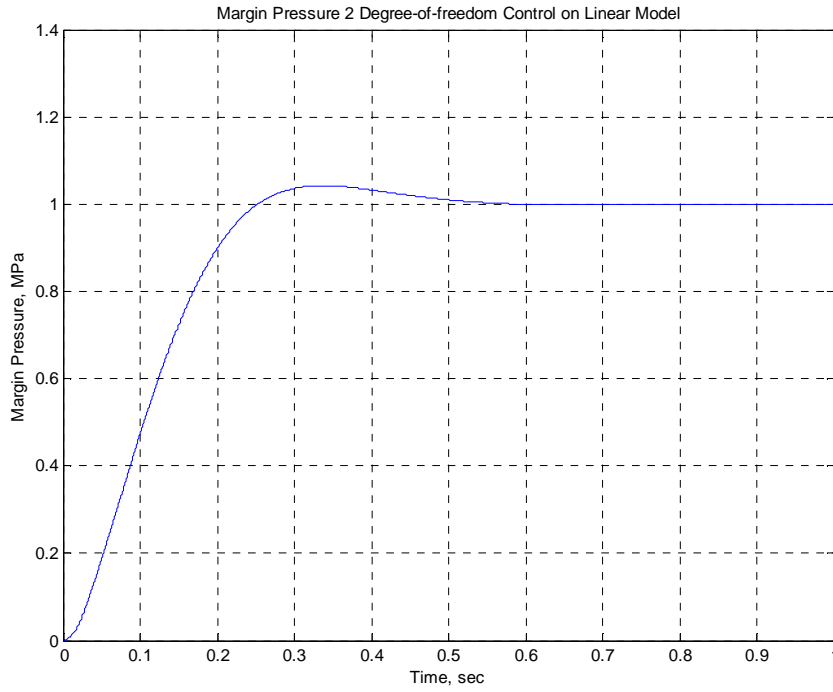


**Fig. 4.5.2 – Margin pressure step response for linear 2 degrees-of-freedom control**

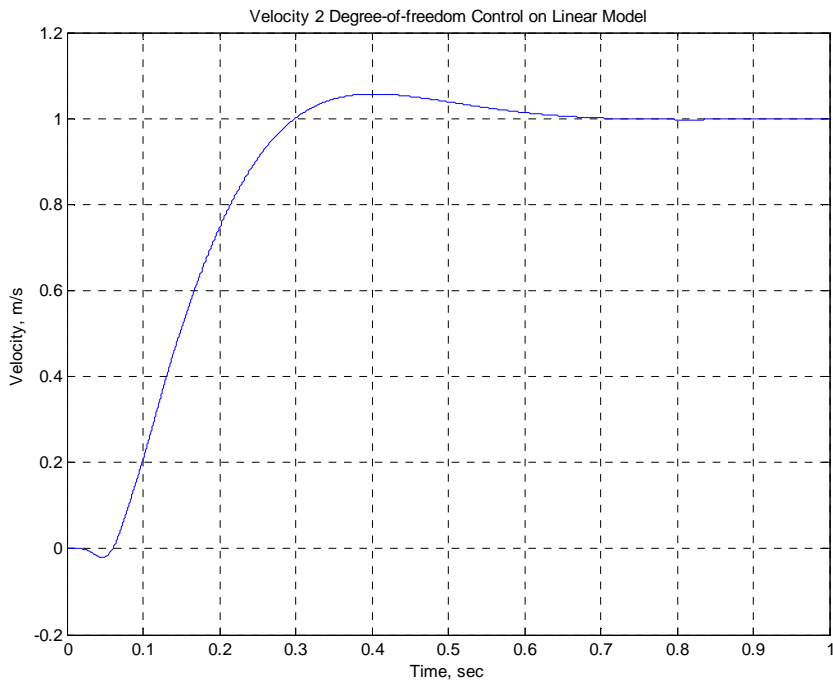


**Fig. 4.5.3 – Velocity step response for linear 2 degrees-of-freedom control**

In both Figures 4.5.2 and 4.5.3, it can be seen that both linear responses closely match the desired closed-loop responses. In both cases, the results are far superior to the responses from the PID controller. In fact, the responses resemble the desired closed-loop performance much more so than the PID design. Both plots do show an increase in overshoot with respect to the desired but the increase does not cause the response to go beyond the performance bounds. The velocity plot, interestingly, shows a bit of the non-minimum phase behavior that is present in the system. The nonlinear results can be seen in Figures 4.5.4 and 4.5.5.

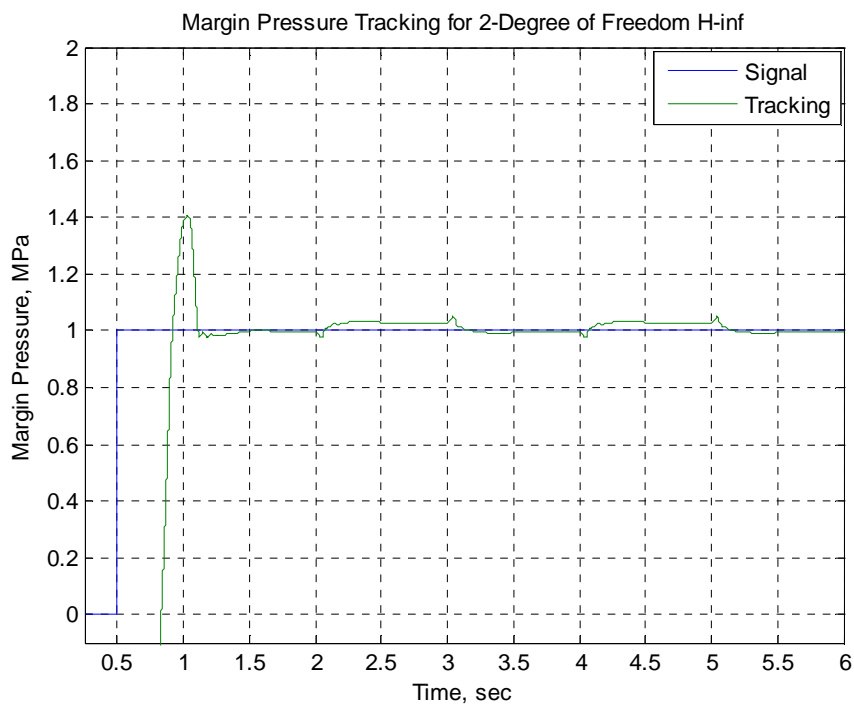


**Fig. 4.5.4 – Margin pressure response for 2 degrees-of-freedom control on the nonlinear model**

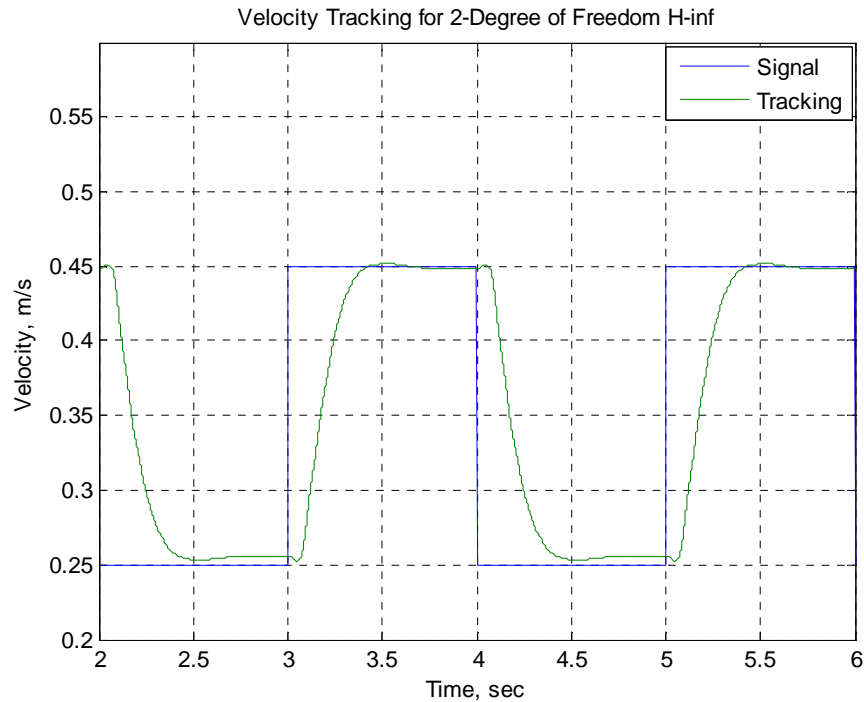


**Fig. 4.5.5 – Velocity response for 2 degrees-of-freedom control on the nonlinear model**

In Figure 4.5.4, it can be seen that margin pressure shows a high degree of decoupling within the system as well as much improved steady-state response. The effects of the velocity modulation can still be seen every second but the effects are greatly reduced compared to the other controllers. In Figure 4.5.5, the velocity performance possesses a fast response time and shows no high frequency oscillations. The response time, however, was not as fast as that of the PID controller, which indicates a slight degradation in performance for an increased amount of robustness. The same non-minimum phase response is present in the nonlinear simulation. In both plots, but in the velocity response most strongly, the desired close-loop response is closely represented.

Once again, this controller is high-order and requires model order reduction similar to both the Mixed Sensitivity and MacFarlane-Glover responses. To show that the

controller is indeed high order, the pz-map of the two degrees-of-freedom controller can be seen in Figure 4.5.6.

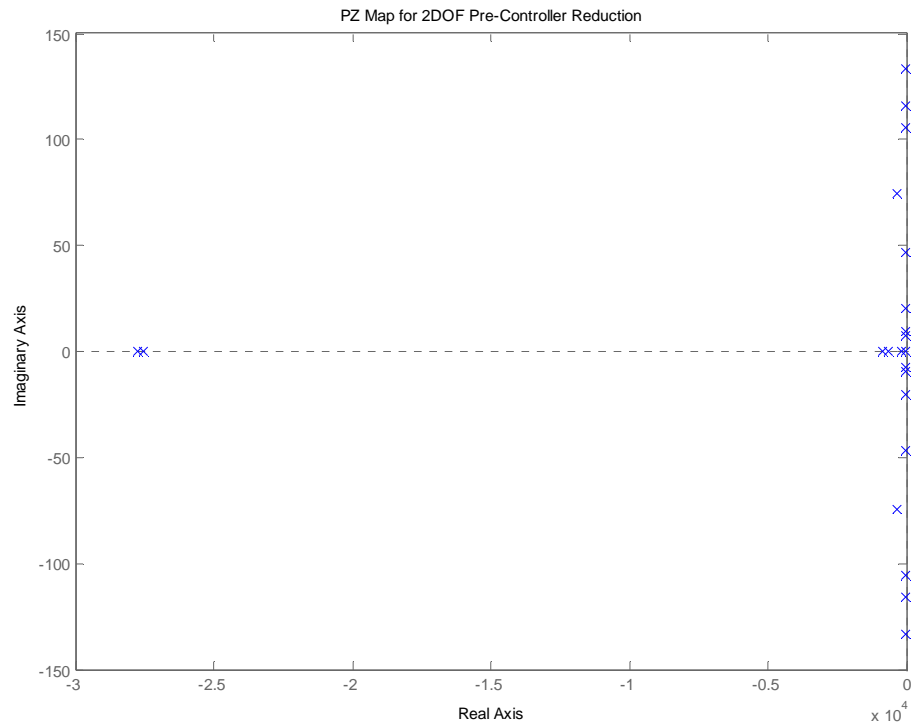


**Fig. 4.5.6 – PZ-map for 2 Degrees-of-freedom controller prior to reduction**

From Figure 4.5.6, it can be seen that the controller exhibits 21 poles with two very fast poles. These commands are very demanding on the system and difficult to achieve.

Also, these poles are very far from the remainder of the poles. These two poles were removed with model order reduction. The pz-map of the reduced controller can be seen in Figure 4.5.7.

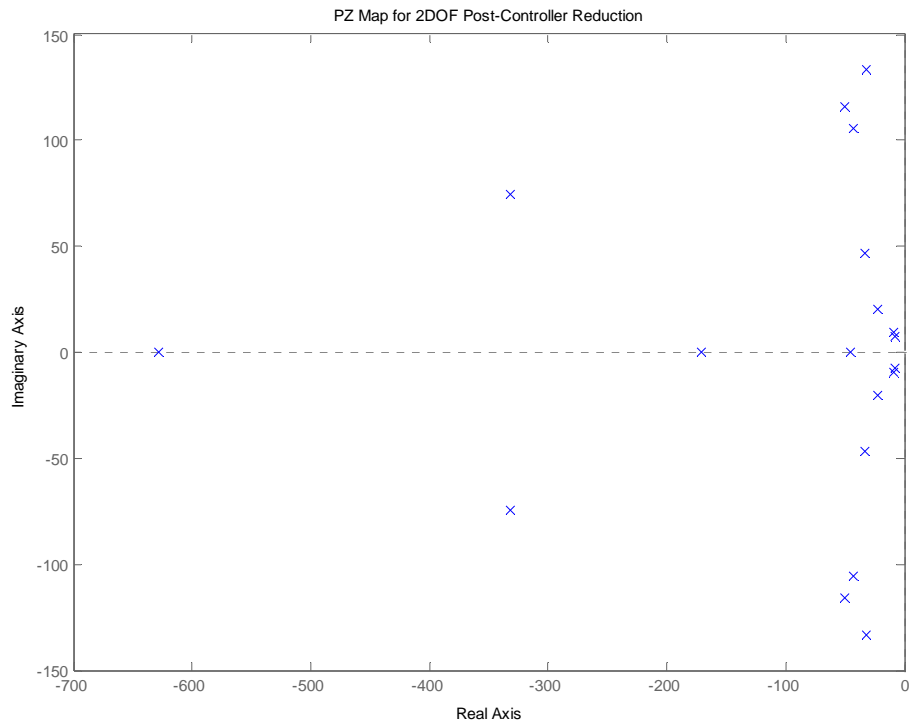


**Fig. 4.5.7 – PZ-map for 2 Degrees-of-freedom controller post reduction**

From Figure 4.5.7, it can be seen that the controller was reduced to 19<sup>th</sup> order and removed the two extremely fast poles. This reduction leaves a controller that, while still having a relatively fast pole at roughly 100 Hz, is far less demanding than the original. The model was reduced to 19<sup>th</sup> order due to it being the smallest order achievable that retained the performance of the controller.



## Chapter 5

### TIME DOMAIN ANALYSIS OF ROBUSTNESS

#### 5.1 Uncertainty Cases

Robustness characteristics can be seen in the time domain. A robust system maintains performance and stability independent of the perturbations or changes in the system dynamics. Perturbations were introduced to each system by applying positive or negative bias. The Positive bias included: +250lbs of bias force, an increase to fluid bulk modulus of +33%, an increase to viscous friction by +25% and an increase of the discharge coefficient by +0.1. The negative case included: -250lbs of bias force, a decrease to fluid bulk modulus of -33%, a decrease to viscous friction by -25% and a decrease of the discharge coefficient by -0.1. These bias values fall within the range of predicted uncertainty outlined in Table 2.4.2. Note that this is just one possible perturbation of the system and is strictly illustrative; other values could have been chosen. The results of this analysis follow.

#### 5.2 Time Domain Responses

The time domain response for each control system can be seen in Figures 5.2.1-5.2.8. It is expected that the PID controller exhibits the worst robustness characteristics while the modern controllers exhibit improved robustness. The PID response will be examined first. In Figure 5.2.1, the margin pressure response for PID can be seen. Also, in Figure 5.2.2, the velocity response for PID can be seen.

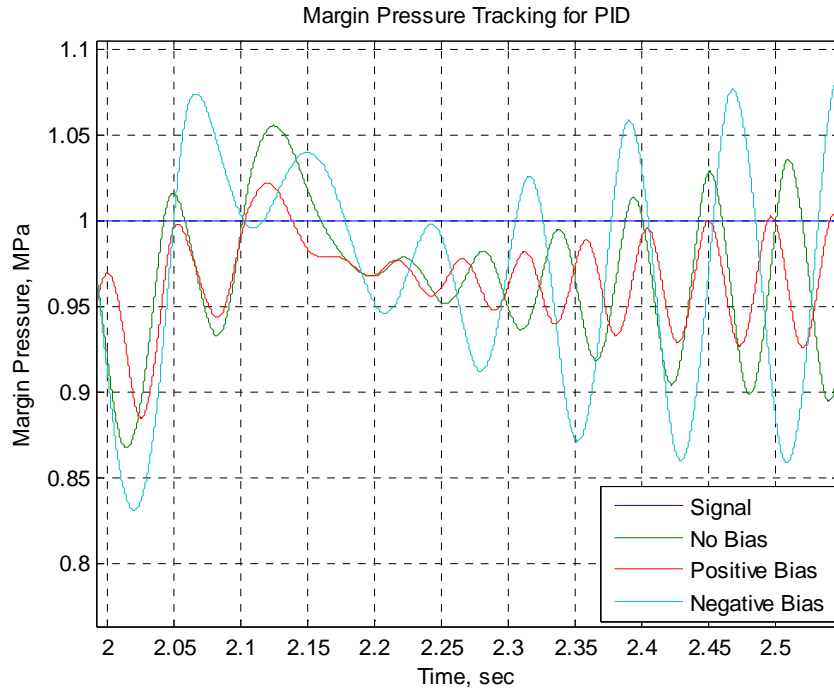


**Fig. 5.2.1 – Margin pressure robustness for PID control**

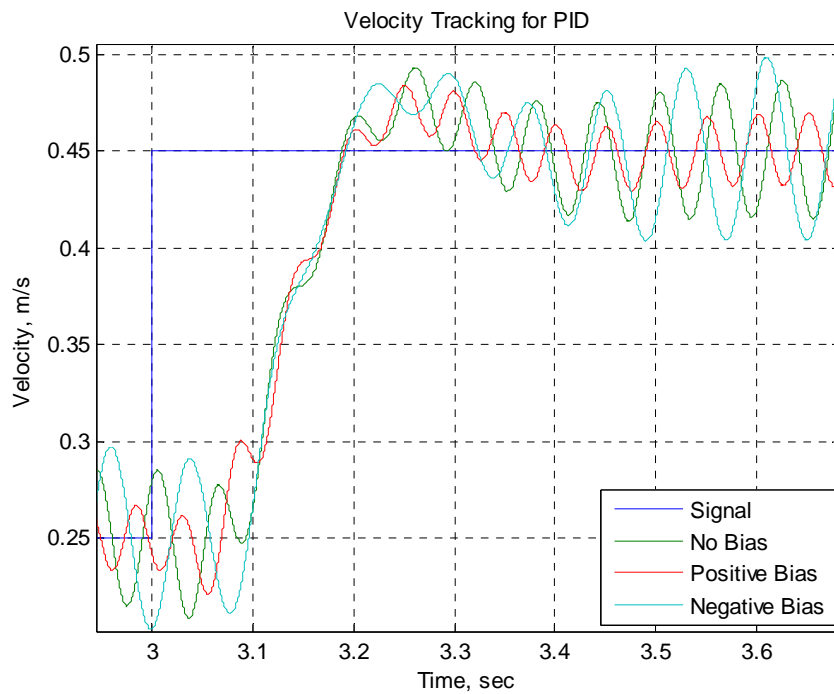


**Fig. 5.2.2 – Velocity robustness for PID control**

From both Fig. 5.2.1 and Fig. 5.2.2, it can be seen that there exists a large degree of variation between the two test cases and the non-biased response. In both outputs, the positive bias force causes the response to show lower oscillation while the negative bias force shows greater tendency towards oscillation and slower response times.

The mixed sensitivity controller response will be examined next. In Figure 5.2.3, the margin pressure response can be seen and in Figure 5.2.4, the velocity response can be seen.

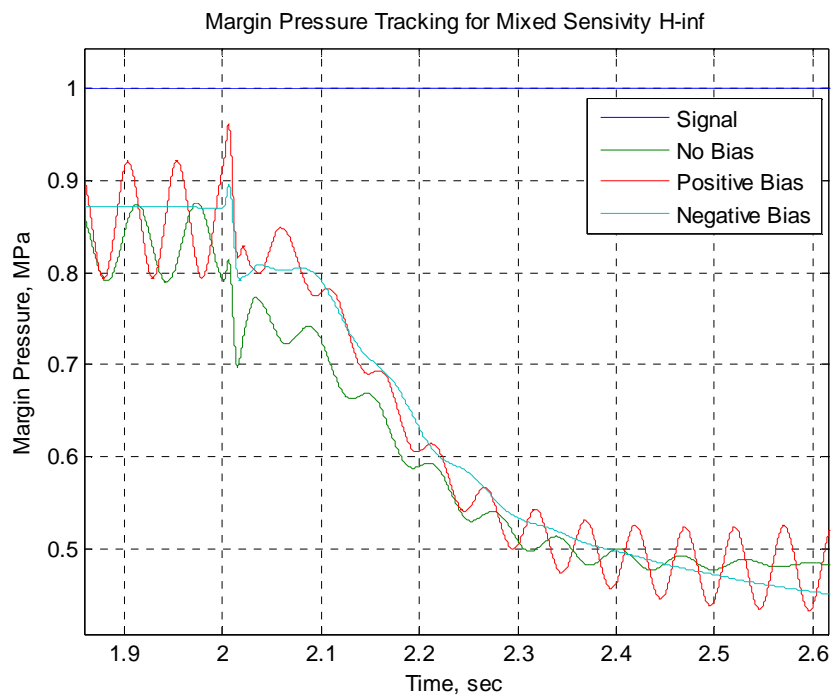


**Fig. 5.2.3 – Margin pressure robustness for the MS controller**

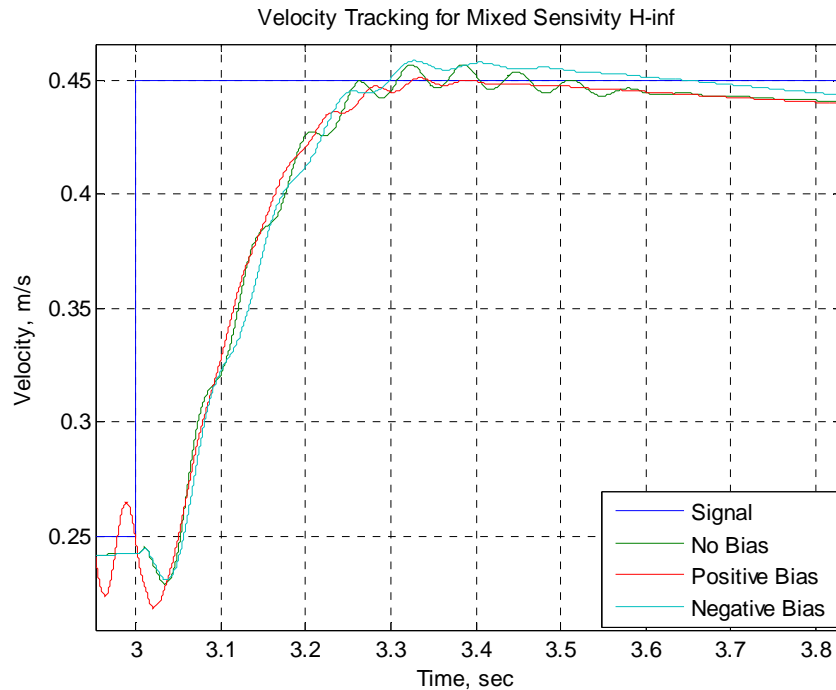


**Fig. 5.2.4 – Velocity robustness for MS controller**

From Figure 5.2.3, it can be seen that the margin pressure shows robustness similar to that of the PID. Though the responses lack the amount of oscillations seen in PID, there is a definite difference between the bias cases. The positive cases make the oscillatory response much worse while the negative bias smooths out. However, in the velocity response from Figure 5.2.4, there is an improvement in robustness. Here too the positive case shows increased oscillation and the negative term shows smoothing but the deviation from the non-biased case is less pronounced.

The MacFarlane-Glover controller is examined next. The margin pressure response can be seen in Figure 5.2.5 while the velocity response can be seen in Figure 5.2.6.

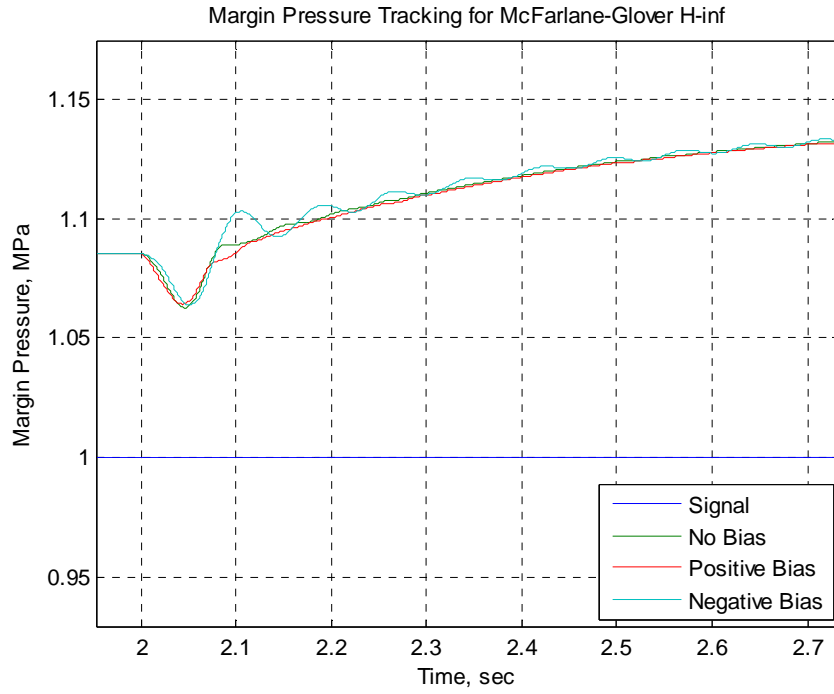


**Fig. 5.2.5 – Margin pressure robustness for MG controller**

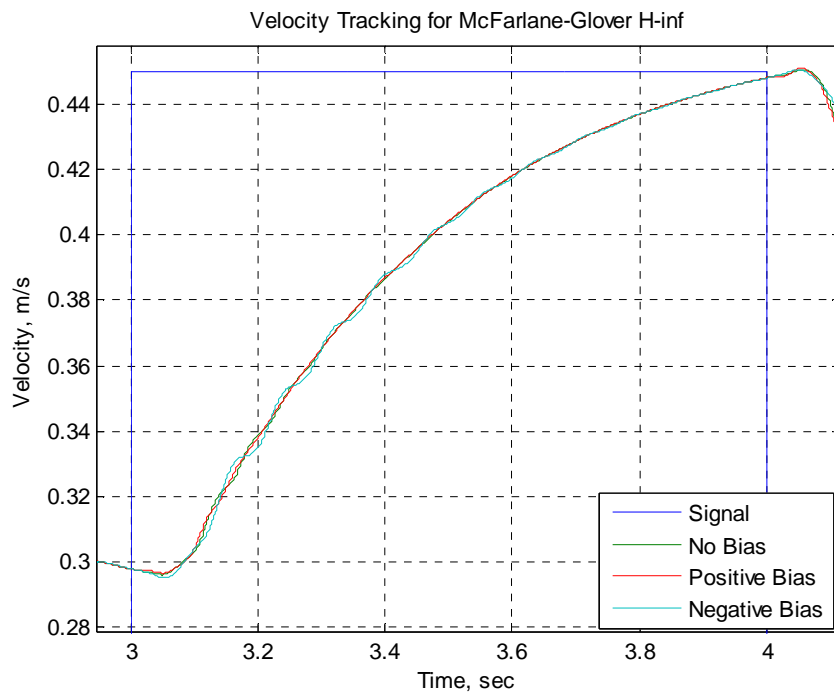


**Fig. 5.2.6 – Velocity robustness for MG controller**

The margin pressure response in Figure 5.2.5 shows greatly improved robustness characteristics compared to the previous two controllers. Here it can be seen that neither the positive nor negative case varies much over the response. The negative bias force shows an increase in oscillations while the positive bias smooths out the response though neither is severe in deviation from the non-biased response. In Figure 5.2.6, a drastic improvement in robustness can be seen. Neither bias case deviates from the non-biased response a significant amount. With respect to the prior two controller schemes, this control shows drastically improved robustness characteristics.

Finally, the two-degree of freedom controller is examined. In Figure 5.2.7, the margin pressure response can be seen, while in Figure 5.2.8, the velocity response can be seen.

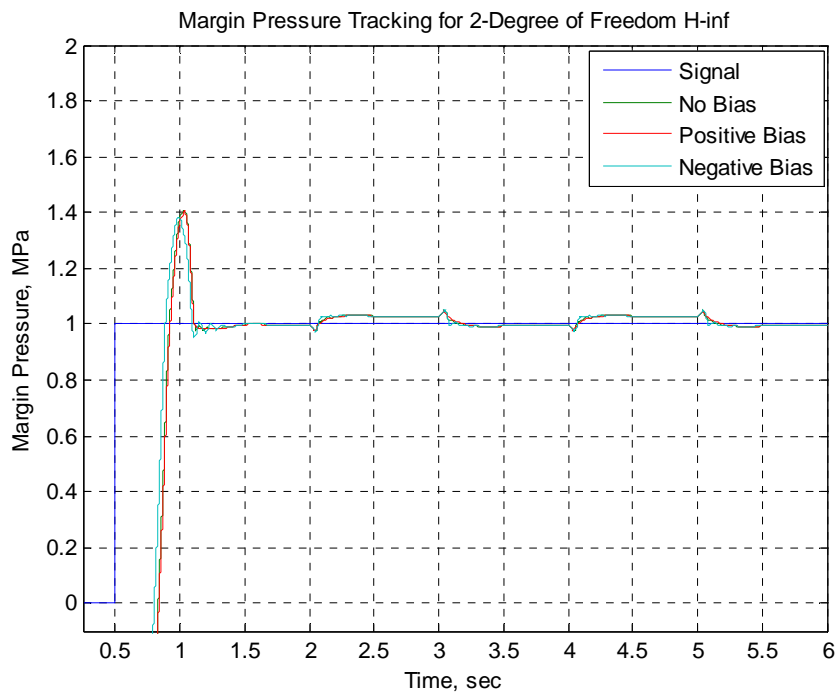


**Fig. 5.2.7 – Margin pressure robustness for 2DOF controller**

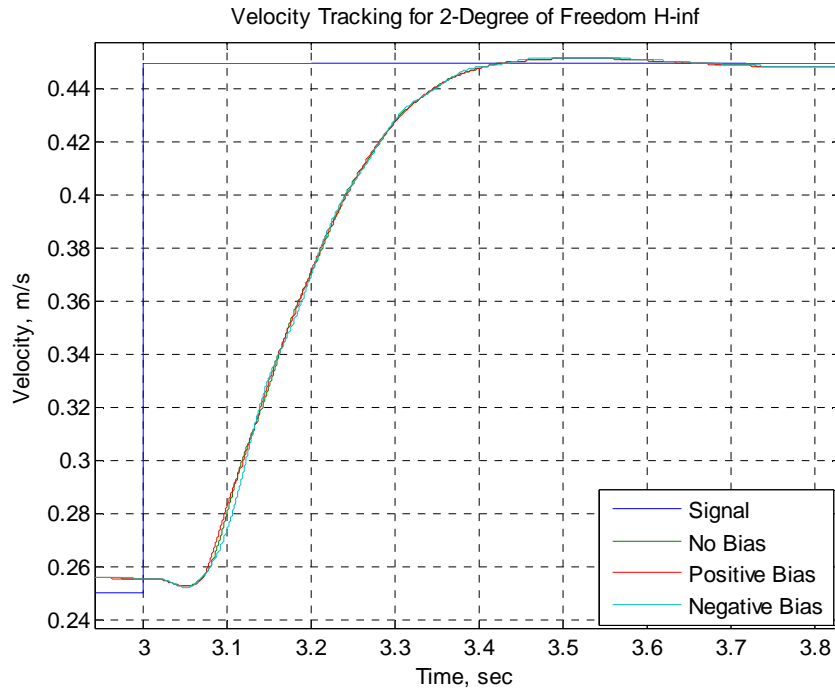


**Fig. 5.2.8 – Velocity robustness for the 2DOF controller**

From Figure 5.2.7, it can be seen that the margin pressure shows very good robustness characteristics. The negative bias case does cause some high frequency oscillations to appear in the result but they are small. This robustness is comparable to the robustness shown in Figure 5.2.5 for the MacFarlane-Glover controller. However, when examining Figure 5.2.8 for velocity response, it can be seen that the robustness characteristics are the best out of all controllers. The time response of the two bias cases for velocity do not show increased oscillation that the other controllers exhibited. Both bias cases show responses that remain very close to the nominal model while also keeping dynamic responses similar.

### **5.3 Time Domain Analysis Conclusions**

The time domain analysis shows that the robustness expectations for the controller systems were accurate. Each modern controller showed progressively improved robustness characteristics over the last while the PID showed the poorest robustness characteristic. Though examining the time domain gives a good indication of relative robustness, it does not show a complete picture. Robustness analysis in the frequency domain provides a much more complete view of how each system will respond under uncertain perturbations.



## Chapter 6

### FREQUENCY DOMAIN ANALYSIS OF ROBUSTNESS

#### 6.1 Frequency Domain Robustness Principles

To evaluate the improved robustness of these controllers more extensively than the time domain analysis,  $H_\infty$  norm analysis techniques are used. These robustness characteristics are defined in four ways: nominal stability, nominal performance, robust stability and robust performance. Nominal stability tests determine whether or not the nominal system is stable without any variation in the system model from nominal. Nominal performance tests determine whether or not the control system with the nominal model meets the desired performance requirements. Robust stability tests determine whether or not the control system is stable for all perturbations of the model in the uncertainty set. Robust performance determines whether or not the performance objective is satisfied for all perturbations of the model in the uncertainty set. All robustness characteristics require that nominal stability holds true. These characteristics are evaluated over a frequency range using the structured singular value of the transfer function matrix. The maximum structured singular value is the  $H_\infty$  norm of the system just as the maximum magnitude of the frequency response of a SISO system is an  $H_\infty$  norm. These criteria are defined using the generalized plant model,  $P$ , and the controller,  $K$ , to create the system matrix,  $N$ . The transformation of  $P$  and  $K$  to  $N$  can be done using a lower linear fractional transformation. This process can be seen visually in Figure 6.1.1.

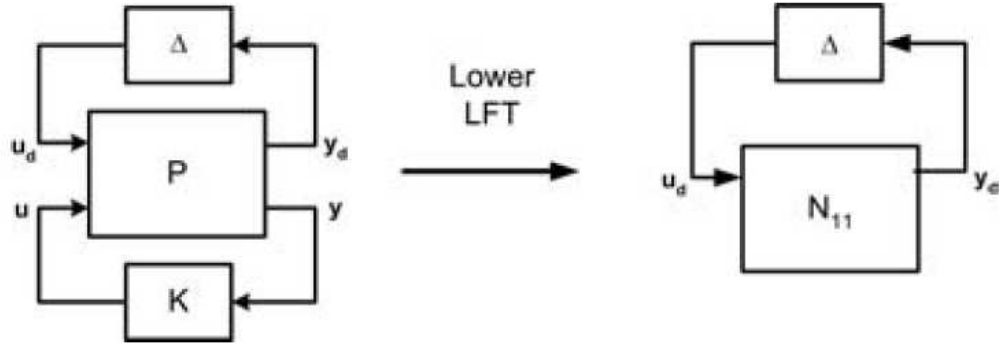


**Fig. 6.1.1 – Transforming P and K into the N-Δ structure [6]**

Mathematically,  $N$  is defined as:

$$N = F_l(P, K) = P_{11} + P_{12}K(I - P_{22}K)^{-1}P_{21} \quad (6.1.1)$$

To define the robustness characteristics, the structured singular value must be presented.

The structured singular value,  $\mu$ , of a plant  $G$  is defined as:

$$\mu_{\Delta}(G) = \frac{1}{\min\{k_m \mid \det(I - k_m G \Delta) = 0 \text{ for structured } \Delta, \bar{\sigma}(\Delta) \leq 1\}} \quad (6.1.2)$$

where  $k_m$  is a scaling factor that makes the matrix  $I - k_m G \Delta$  singular. The robustness definitions to be applied to each control system are derived in Skogestad and Postlethwaite. The following equations are the robustness characteristics used for analysis in this research:

$$NS: N \text{ is stable internally} \quad (6.1.3)$$

$$NP: \bar{\sigma}(N_{22}) = \mu_{\Delta p} < 1 \quad \forall \omega \quad (6.1.4)$$

$$RS: \mu_{\Delta}(N_{11}) < 1 \quad \forall \omega \quad (6.1.5)$$

$$RP: \mu_{\Delta}(N(j\omega)) < 1 \quad \forall \omega \quad (6.1.6)$$

To satisfy all robustness parameters, each value must be below 1 (absolute) or 0 dB over all frequencies. Nominal stability was determined during the control design phase by examining the closed-loop pole locations. The stable responses in the time domain analysis confirm nominal stability. As discussed in Chapter 2, the uncertainty for the system is modeled as output multiplicative uncertainty.

## 6.2 Applying Robust Analysis to PID

To apply robust analysis, the system must be modified by adding an uncertainty model, as seen in Figure 2.4.1. The generalized plant  $P$  is defined for each system. For the control structure outlined in Chapter 4.2, the generalized plant is:

$$P = \begin{bmatrix} 0 & 0 & w_o G_s \\ w_p & -w_p & -w_p G_s \\ I & -I & -G_s \end{bmatrix} \quad (6.2.1)$$

where  $G_s$  is the shaped plant,  $w_o$  is the output uncertainty and  $w_p$  is the performance weight. This process can be seen in Appendix D. In Figure 6.2.1, the robustness norms are plotted for PID control.

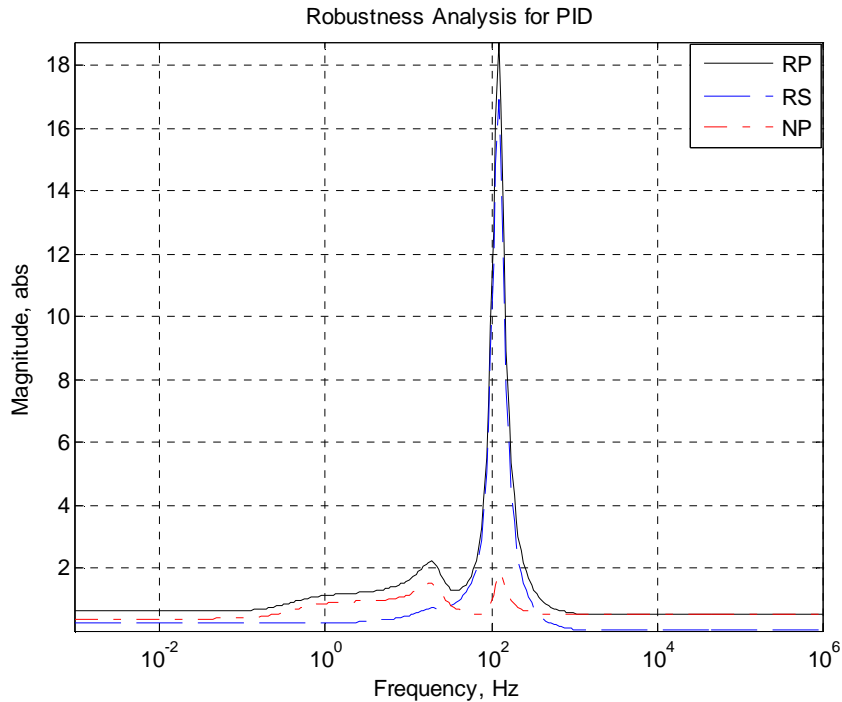


**Fig. 6.2.1 – Robustness analysis for PID controller**

It can be seen from Figure 6.2.1 that PID control does not satisfy the robustness criterion. Nominal performance peaks at 1.9, robust stability peaks at 17.0 and robust performance peaks at 19.0. This information means that the selected PID controller will not perform to the desired specifications under all plant model perturbations and that some plant perturbation exists that will cause the system to become unstable.

### 6.3 Applying Robust Analysis to Mixed Sensitivity Control

The generalized plant for the mixed sensitivity controller is identical to that of the PID controller because they both have the same control structure; Eq. (6.2.1) is the generalized plant for this analysis. The robustness characteristics of mixed sensitivity controller can be seen in Figure 6.3.1.

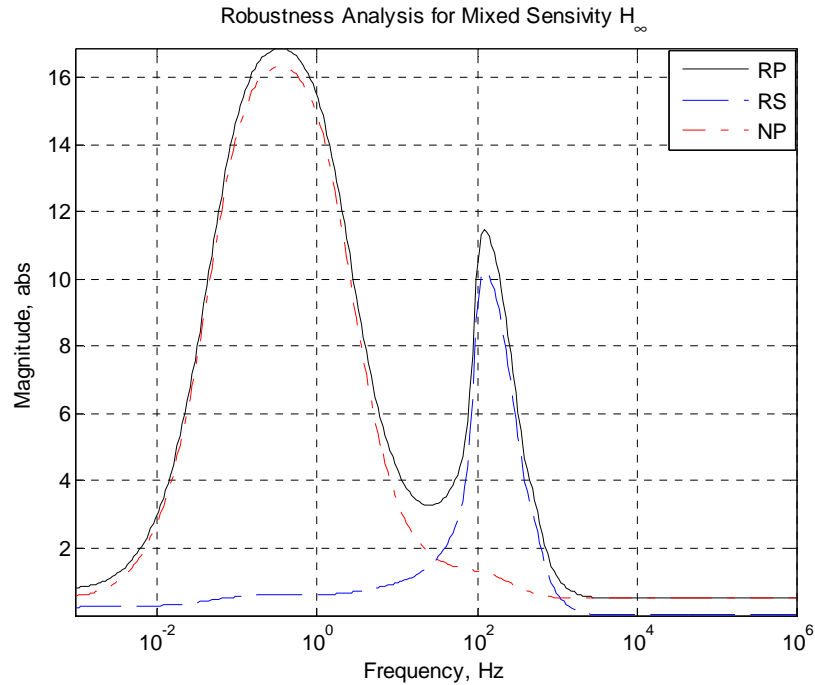


**Fig. 6.3.1 – Robustness analysis for the mixed sensitivity controller**

From Figure 6.3.1, it can be seen that mixed sensitivity showed improved robustness in some aspects, but also shows a higher peak in the nominal performance. Nominal performance peaks at 16.3, robust stability peaks at 10.3 and robust performance peaks at 16.9. The nominal performance peak is consistent with the poor decoupling and poor tracking in the margin pressure. However, despite the setback in nominal performance, both of the remaining robustness characteristics showed improvement over the PID controller.

## 6.4 Applying Robust Analysis for MacFarlane-Glover $H_\infty$ Loop-shaping Control

The generalized plant for robustness analysis for MacFarlane-Glover  $H_\infty$  Loop-shaping control can be seen as:

$$P = \begin{bmatrix} 0 & 0 & w_o G_s \\ -w_p & w_p & w_p G_s \\ -I & I & G_s \end{bmatrix} \quad (6.4.1)$$

This process can be seen in Appendix D. Plots of the robustness characteristics can be seen in Figure 6.4.1.

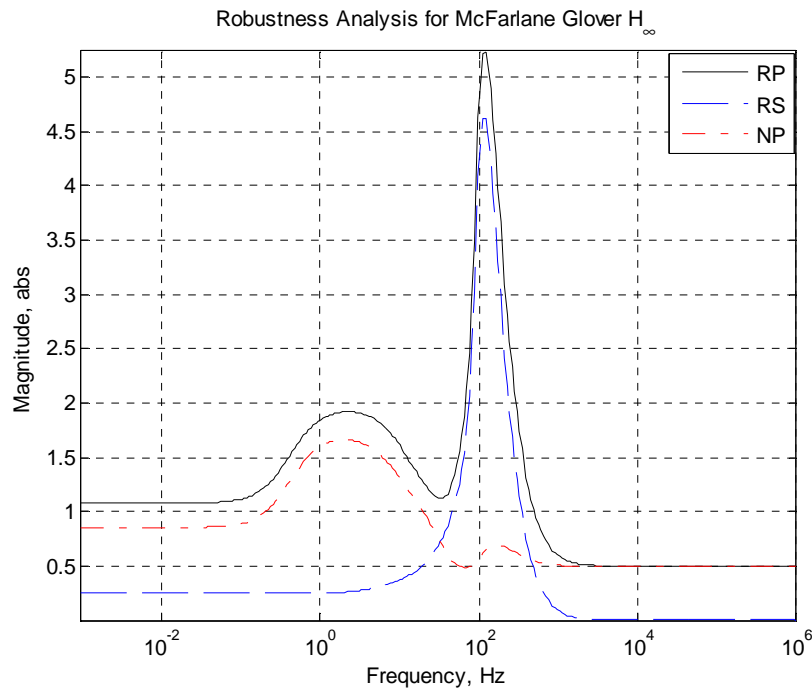


**Fig. 6.4.1 – Robustness analysis for MacFarlane-Glover  $H_\infty$  loop-shaping control**

From Figure 6.4.1, it can be seen that MacFarlane-Glover showed improved robustness in all aspects despite poor performance in velocity control in the time domain simulations. Nominal performance peaks at 1.7, robust stability peaks at 4.7 and robust performance peaks at 5.3. These results are significantly better than the original PID control while also being superior to mixed sensitivity.

## 6.5 Applying Robust Analysis for Two Degree-of-Freedom $H_\infty$ Loop-shaping

### Control

The generalized plant for two degree-of-freedom  $H_\infty$  loop-shaping control is defined as:

$$P = \begin{bmatrix} 0 & 0 & w_o G_s \\ w_p & -w_p & -w_p G_s \\ I & 0 & 0 \\ 0 & I & G_s \end{bmatrix} \quad (6.5.1)$$

This process can be seen in Appendix D. Figure 6.5.1 shows the set of plots for the robustness parameters for the two degree-of-freedom controller scheme.

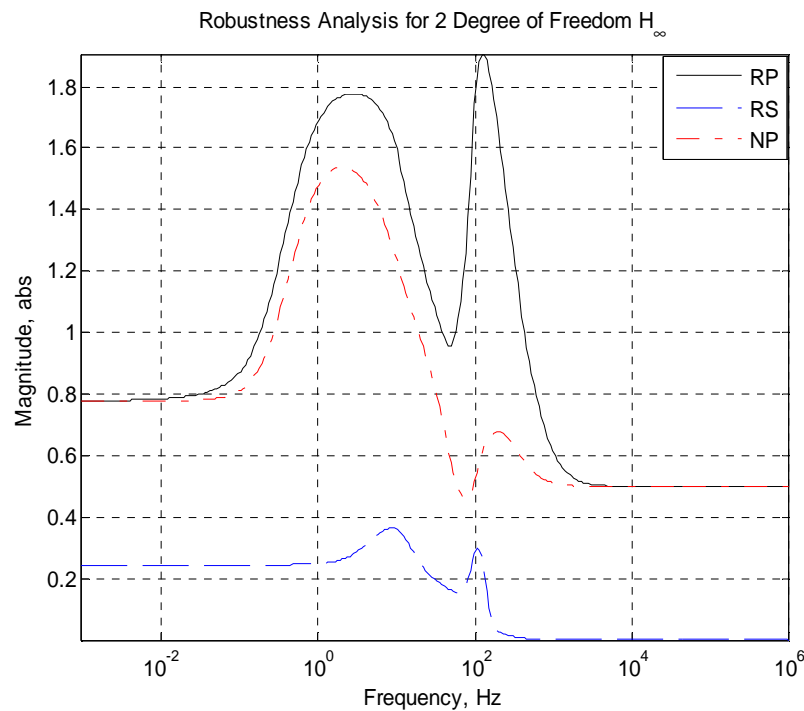


**Fig. 6.5.1 - Robustness Analysis for two degrees-of-freedom  $H_\infty$  Loop-shaping control**

From Figure 6.5.1, it can be seen that the two degree-of-freedom system shows great improvements over all the previous controllers. Nominal performance peaks at 1.5,

robust stability peaks at 0.4 and robust performance peaks at 1.9. It should be noted that this is the only system to successfully satisfy robust stability which is significant. This implies that for any possible plant perturbation that was modeled, the system will be stable.

## 6.6 Robustness Conclusions

From the previous analysis, it was shown that robustness characteristics associated with the modern controllers were superior to PID. The results of this analysis can be summarized in Table 6.6.1.

*Table 6.6.1 Summary for frequency domain robustness analysis*

	Peak Value (absolute)		
	Nominal Performance	Robust Stability	Robust Performance
PID	1.9	17.0	19.0
Mixed Sensitivity $H_{\infty}$	16.3	10.3	16.9
MacFarlane-Glover $H_{\infty}$ Loop-Shaping	1.7	4.7	5.3
Two Degree-of-Freedom $H_{\infty}$ Loop-Shaping	<b>1.5</b>	<b>0.4</b>	<b>1.9</b>

From Table 6.6.1, it can be seen that these modern control candidates show improved robust stability and improved robust performance over that of the PID controller. Also, with the exception of MS control, even nominal performance is improved.



These controllers are able to satisfy neither nominal performance nor robust performance, but it can be seen that these modern control candidates show a trending that moves towards satisfying robustness characteristics. From these results, it shows that the more advanced controllers are able to handle more cases of perturbation. The results of the frequency domain analysis support what was seen in the time domain analysis. In the time domain all the test case perturbations were stable, though the frequency domain analysis shows that only one controller is robustly stable. This is not contradictory, but instead means the two perturbation cases used for the time analysis existed inside the set of possible models that would remain stable for the controllers.

## Chapter 7

### CONCLUSIONS

#### 7.1 Overview

As seen from the work on this project, the ability of modern controllers to provide improved performance and robustness for an uncertain hydraulic system was very good. The controllers, for the most part, improved performance and also improved robustness. In the time domain, it was observed that the modern controllers provided improved robustness to plant perturbations compared to the PID as seen in Figures 5.2.1-5.2.8. Performance was sacrificed on the mixed-sensitivity controller and also on the MacFarlane-Glover controller for the sake of robustness, which was expected to some degree. With respect to decoupling the system, the modern controllers did a better job than the PID for all cases except the mixed-sensitivity controller.

Overall the two degrees-of-freedom controller showed the best improvement in robustness without sacrificing performance as seen in Table 6.6.1. There are several advantages that are garnered by the two degrees-of-freedom controller. It possesses the best robustness characteristics and performance out of all the controllers tested. The closed-loop characteristics can be designed directly into the controller via the reference input modeling, which allows the designer better control over the dynamics of the system. The two degrees-of-freedom controller also proved to be the easiest of all the controllers to design.

## **7.2 Limitation of $H_{\infty}$ Control**

However, there are drawbacks to these controller schemes. For every controller algorithm, higher-order controllers were produced which could have high demands for the processor both during design and simulation and for onboard processors running the controller. Model reduction can alleviate some of the demand on the processors but that is another step in design that takes an iterative process to determine, which equates to longer design times. The controllers also require the knowledge of a system plant model to design the controller. This would prove difficult to achieve if a system is not well known or not well modeled. Tuning the controller in-the-field would require knowledge of the controller algorithm and additional processing power.

## **7.3 Scope of Future Work**

Future work for this research includes testing the controllers on hardware and evaluating the appropriateness on real industrial machines. Furthermore, the controller can be expanded to handle all four valves independently so that operating conditions such as regenerative flow could be evaluated.

## Appendix A

### MATLAB CODE FOR MIXED SENSITIVITY

For mixed sensitivity design, the methodology outlined in Chapter 3.3 was used. In that section, the terms  $S$  and  $SK$  were identified as important design aspects for this system.

This reduces the quantities to minimize in design as:

$$\left\| \begin{array}{c} S w_p \\ SK w_u \end{array} \right\|_{\infty}$$

To apply this control to a MIMO system, a matrix of weights was chosen for each input.

The 2x2  $w_p$  and  $w_u$  matrices are assembled.

```
%%H-infinity mixed sensitivity%%%%%%%%%%
% 1 - Margin Pressure
% 2 - Velocity Control
A_1 = .1;
A_2 = .05;
bandwidth_1 = .001*2*pi;
bandwidth_2 = .8*pi*2;
M_1 = 10;
M_2 = 2;

w_p1 = tf([1/M_1 bandwidth_1], [1 bandwidth_1*A_1]);
w_p2 = tf([1/M_2 bandwidth_2], [1 bandwidth_2*A_2])

muv=1/100;
numu=[muv];
denu=[0 1];
sysWu=tf(numu,denu);

numu=[muv];
denu=[0 1];
sysWu2=tf(numu,denu);
w_u=[sysWu 0;0 sysWu2];

w_p=[w_p1 0;0 w_p2]
```

The gearalized plant for controller design is

$$P = \begin{bmatrix} w_p & -w_p G \\ 0 & w_u \\ I & -G \end{bmatrix}$$

$P$  is found via block diagram reduction outlined in section 3.3. The generalized plant is packed and the values for design are sent to *hinfsyn.m* from the mu analysis and synthesis Matlab tool box [9].  $gmin$  = minimum gamma value,  $gmax$  = maximum gamma value,  $tol$  = tolerance. The returned controller is unpacked, transformed into a state-space representation

```
dim=2;
P_hinf=[w_p -w_p*Gs;
0*eye(dim) w_u;
eye(dim) -Gs];

ssP=minreal(ss(P_hinf));
[aP,bP,cP,dP]=ssdata(ssP);
pckP=pck(aP,bP,cP,dP);
qt=1;gmin=0.1;gmax=15;tol=1e-3;epr=1e-12;epp=1e-8;rm=2;
nc_hinf=dim;nm=dim;
[Khinf,cl,gf,ax,ay,hx,hy]=hinfsyn(pckP,nm,nc_hinf,gmin,gmax,tol,rm,epr,epp,qt);

[aK,bK,cK,dK]=unpck(Khinf);
ssK=ss(aK,bK,cK,dK);
```

Due to the high order of the controller,  $K$ , there were many fast poles that affected performance and simulation. To reduce these problems, a model reduction method found on page 466 of Skogestad [2] was used. It requires an iterative process dropping the order so that the dimensions are as small as possible but still stable. In this case, the system was reduced to 13<sup>th</sup> order.

```
%Model Reduction Page 466 Skogestad
sysred=pck(ssK.a,ssK.b,ssK.c,ssK.d);
sysd=strans(sysred);
syst=strunc(sysd,13);
sysr=sresid(sysd,13);
```

```
[asysr,bsysr,csysr,dsysr]=unpck(sysr);
tfK=ss(asysr,bsysr,csysr,dsysr);
```

To test for nominal performance and robust performance, performance requirements must be laid out

```
% 1 - Margin Pressure
% 2 - Velocity Control
M_1 = 2; % *100%
bandwidth_1 = 2*pi*2;
A_1 = .15; % *100%

M_2 = 2;
bandwidth_2 = 1.5*pi*2;
A_2 = .05;

w_p1 = tf([1/M_1 bandwidth_1], [1 bandwidth_1*A_1]);
w_p2 = tf([1/M_2 bandwidth_2], [1 bandwidth_2*A_2]);

w_p(1,1) = w_p1;
w_p(2,2) = w_p2;
w_p(1,2)=0;
w_p(2,1)=0;
```

To determine robust characteristics, the plant matrix  $N$  is formed.  $P$ , the generalized plant model, is defined for output uncertainty. That matrix is:

$$P = \begin{bmatrix} 0 & 0 & w_o G_s \\ w_p & -w_p & -w_p G_s \\ I & -I & -G_s \end{bmatrix}$$

In this form,  $w_p$  is the matrix of performance requirements,  $w_o$  is the uncertainty bound and  $G_s$  is the plant. The matrix is turned into  $N$  via the linear fractional transformation which can be compiled using the Matlab function, `lft.m` using the matrix  $P$  and the controllers. The code ends with the code used to plot the robustness specifications.

Dimensions are 2x2 hence `dim=2`. `WaSS` is `w_o` in the code.

```

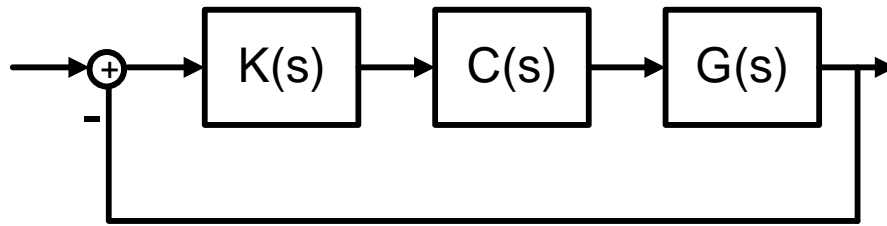
P=[eye(dim,dim)*0 eye(dim,dim)*0 WaSS*Gs; w_p -w_p -w_p*Gs; eye(dim,dim) -
eye(dim,dim) -Gs];
N=lft(P,tfK);
N=pck(N.a,N.b,N.c,N.d); %competes the packed form
Nf = frsp(N,w);          %examines the frequency response over the frequency
% mu for RP
blk = [2 2; 2 2]; %creates the block for the mu command
[mubnds,rowd,sens,rowp,rowg] = mu(Nf,blk,'c'); %calculates the structured singular
value
muRP = sel(mubnds,':',1); % selects the correct structured value
pkvnorm(muRP) %computes the norm of the condition
% mu for RS
Nrs=sel(Nf,1:2,1:2); [mubnds,rowd,sens,rowp,rowg]=mu(Nrs,[2 2],'c');
muRS = sel(mubnds,':',1); pkvnorm(muRS)
% mu for NP (= max. singular value of Nnp)
Nnp=sel(Nf,3:4,3:4); [mubnds,rowd,sens,rowp,rowg]=mu(Nnp,[2 2],'c');
muNP = sel(mubnds,':',1); pkvnorm(muNP)

figure(45)
semilogx(muRP(1:end-1,2),muRP(1:end-1,1),'-k');
hold on
semilogx(muRS(1:end-1,2),muRS(1:end-1,1),'--b')
semilogx(muNP(1:end-1,2),muNP(1:end-1,1),'-r')
hold off
grid, xlabel('Frequency, Hz'), ylabel('Magnitude, abs')
legend('RP','RS','NP')
axis tight
title('Robustness Analysis for Mixed Sensitivity  $H_{\infty}$ ')

```

## Appendix B

### MATLAB CODE FOR MACFARLANE-GLOVER LOOP-SHAPING



MacFarlane-Glover (MG)  $H_\infty$  loop shaping utilizes a PID design for performance and creates a controller that improves robustness. This controller bridges the gap between SISO PID design and MIMO  $H_\infty$  robust control design. The plant  $L$  is the shaped-plant. *coprimeunc.m* is an m-file from Skogestad and Postlethwaite found on [10].

```
L=Gs*comp;  
gamrel=1.00000001;  
[Ac,Bc,Cc,Dc,gammin]=coprimeunc(L.a,L.b,L.c,L.d,gamrel);
```

Due to the high order of the controller,  $K$ , there were many fast poles that affected performance and simulation. To reduce these problems, a model reduction method found on page 466 of Skogestad [2] was used. It requires an iterative process dropping the order so that the dimensions are as small as possible but still stable. In this case, the system was reduced to 16<sup>th</sup> order.

```
%Model Reduction Page 466 Skogestad  
sysred=pck(Ac,Bc,Cc,Dc);  
sysd=strans(sysred);  
syst=strunc(sysd,16);  
sysr=sresid(sysd,16);  
[Ac,Bc,Cc,Dc]=unpck(sysr);
```



To test for nominal performance and robust performance, performance requirements must be laid out

```
% 1 - Margin Pressure
% 2 - Velocity Control
M_1 = 2; % *100%
bandwidth_1 = 2*pi*2;
A_1 = .15; % *100%

M_2 = 2;
bandwidth_2 = 1.5*pi*2;
A_2 = .05;

w_p1 = tf([1/M_1 bandwidth_1], [1 bandwidth_1*A_1]);
w_p2 = tf([1/M_2 bandwidth_2], [1 bandwidth_2*A_2]);

w_p(1,1) = w_p1;
w_p(2,2) = w_p2;
w_p(1,2)=0;
w_p(2,1)=0;
```

To determine robust characteristics, the plant matrix  $N$  is formed.  $P$ , the generalized plant model, is defined for output uncertainty. That matrix is:

$$P = \begin{bmatrix} 0 & 0 & w_o G_s \\ -w_p & w_p & w_p G_s \\ -I & I & G_s \end{bmatrix}$$

In this form,  $w_p$  is the matrix of performance requirements,  $w_o$  is the uncertainty bound and  $G_s$  is the plant. The matrix is turned into  $N$  via the linear fractional transformation which can be compiled using the Matlab function, `lft.m` using the matrix  $P$  and the controllers. The code ends with the code used to plot the robustness specifications.

Dimensions are 2x2 hence `dim=2`. `WaSS` is  $w_o$  in the code.

```
dim=2;
P=[eye(dim,dim)*0 eye(dim,dim)*0 WaSS*Gs; -w_p w_p w_p*Gs; -eye(dim,dim)
eye(dim,dim) Gs]; %creates the generalized plant
```

```

N=lft(P,W1*sys_mac);
N=pck(N.a,N.b,N.c,N.d); %competes the packed form
Nf = frsp(N,w);          %examines the frequency response over the frequency
% mu for RP
blk = [2 2; 2 2]; %creates the block for the mu command
[mubnds,rowd,sens,rowp,rowg] = mu(Nf,blk,'c'); %calculates the structured singular
value
muRP = sel(mubnds,':',1); % selects the correct structured value
pkvnorm(muRP) %computes the norm of the condition
% mu for RS
Nrs=sel(Nf,1:2,1:2); [mubnds,rowd,sens,rowp,rowg]=mu(Nrs,[2 2],'c');
muRS = sel(mubnds,':',1); pkvnorm(muRS)
% mu for NP (= max. singular value of Nnp)
Nnp=sel(Nf,3:4,3:4); [mubnds,rowd,sens,rowp,rowg]=mu(Nnp,[2 2],'c');
muNP = sel(mubnds,':',1); pkvnorm(muNP)

```

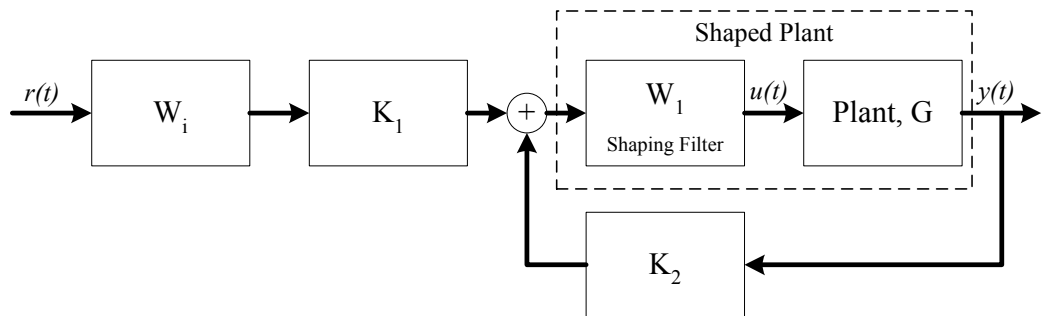
```

figure(43)
semilogx(muRP(1:end-1,2),muRP(1:end-1,1),'-k')
hold on
semilogx(muRS(1:end-1,2),muRS(1:end-1,1),'--b')
semilogx(muNP(1:end-1,2),muNP(1:end-1,1),'-r')
hold off
grid, xlabel('Frequency, Hz'), ylabel('Magnitude, abs')
legend('RP','RS','NP')
axis tight
title('Robustness Analysis for McFarlane Glover  $H_{\infty}$ ')

```

## Appendix C

### MATLAB CODE FOR TWO DEGREES-OF-FREEDOM LOOP-SHAPING



Designing the 2 degrees-of-freedom  $H_\infty$  Loop-shaping controller uses the Matlab code laid out. Each step of code and how to use it will be explained in detail.  $W_i$  is the PID controller designed for performance for the closed loop system. Creating this controller is done by following standard PID design methods. Select the desired closed-loop transfer function  $T_{ref}$  between the commands and controlled inputs. This code section uses standard second order dynamic transfer functions that specify dynamic performance for each reference input, margin pressure and velocity.

```

wn_p=2.1*2*pi; m % Natural frequency for margin pressure
zeta_p=0.7;      % Damping ratio for margin pressure
wn_v=1.7*2*pi; % Natural frequency for velocity
zeta_v=0.7;     % Damping ratio for velocity
Tref11 = tf([wn_p^2],[1 2*zeta_p*wn_p wn_p^2]); % Margin pressure reference model
Tref22 = tf([wn_v^2],[1 2*zeta_v*wn_v wn_v^2]); % Velocity reference model
Tref=ss([Tref11 0;0 Tref22]);

```

The algorithm that will derive the optimized controller requires that the shaped plant,  $G*W_i$ , and the desired closed-loop transfer function,  $T_{ref}$ , be in the packed matrix form.

```

G_shaped = Gs*W1; % shaped plant
Gs_pck = pck(G_shaped.a, G_shaped.b, G_shaped.c, G_shaped.d); %convert into
packed form

```

```
Tref_pck = pck(Tref.a, Tref.b, Tref.c, Tref.d); %convert into packed form
```

$\rho$  is set to a value between 1 and 3. This parameter is a scalar value that lets the designer determine emphasis on model matching in the optimization at the expense of robustness. Increasing  $\rho$  will place more emphasis on model matching.

```
rho=1.1;
```

With the shaped plant, the desired closed-loop matrix and  $\rho$ , the optimization is run to determine the controller. The Matlab file 'hinf2dof' can be found on [11].

This file is simply the optimization routine used to find the controller. To use the controller, it should be unpacked and, in this case, turned into state-space.

```
K_2dof_pck=hinf2dof(Gs_pck, Tref_pck, rho);  
[Ak2dof, Bk2dof, Ck2dof, Dk2dof]=unpck(K_2dof_pck);  
K_2dof=ss(Ak2dof, Bk2dof, Ck2dof, Dk2dof);
```

Due to the high order of the controller,  $K$ , there were many fast poles that affected performance and simulation. To reduce these problems, a model reduction method found on page 466 of Skogestad [2] was used. It requires an iterative process dropping the order so that the dimensions are as small as possible but still stable. In this case, the system was reduced to 19<sup>th</sup> order.

```
sysred=pck(K_2dof.a, K_2dof.b, K_2dof.c, K_2dof.d);  
sysd=strans(sysred);  
sysr=sresid(sysd, 19);  
[asysr, bsysr, csysr, dsysr]=unpck(sysr);
```

```
K_2dof=ss(asysr,bsysr,csysr,dsysr);
```

The controller given by the optimization is a meshing of  $K_1$  and  $K_2$ . The model calls for two controller gains, one for the feedback and one for the reference transfer functions.

Because there are 2 inputs and 2 outputs,  $K$  had dimensions of 2x4. The upper quadrant is  $K_1$  while the lower is  $K_2$ . Therefore, the controller was split into two 2x2 controllers.

$W_i$  is created by looking at the DC gain of the closed loop system and the reference transfer function. This code is directly a translation of the equation:

$$W_i = \left[ (I - G_{S,0} K_{2,0})^{-1} G_{S,0} K_{1,0} \right]^{-1} T_{ref,0}$$

The code follows:

```
K1=K_2dof(:,1:2); K2=K_2dof(:,3:4); %extract K1 and K2
Hinf2dof_cl=series(K1,feedback(G_shaped,-K2)); %form closed-loop system for Wi
Wi_2dof=inv(dcgain(Hinf2dof_cl))*dcgain(Tref); % calculate Wi
```

To test for nominal performance and robust performance, performance requirements must be laid out

```
%1 - Margin Pressure
%2 - Velocity Control
M_1 = 2; % *100%
bandwidth_1 = 2*pi*2;
A_1 = .15; % *100%
M_2 = 2;
bandwidth_2 = 1.5*pi*2;
A_2 = .05;
w_p1 = tf([1/M_1 bandwidth_1], [1 bandwidth_1*A_1]); %form performance weight
TFs
w_p2 = tf([1/M_2 bandwidth_2], [1 bandwidth_2*A_2]); %form performance weight
TFs
w_p(1,1) = w_p1;
w_p(2,2) = w_p2;
```

```
w_p(1,2)=0;
w_p(2,1)=0;
```

To determine robust characteristics, the plant matrix  $N$  is formed.  $P$ , the generalized plant model, is defined for output uncertainty. That matrix is:

$$P = \begin{bmatrix} 0 & 0 & w_o G_s \\ w_p & -w_p & -w_p G_s \\ I & 0 & 0 \\ 0 & I & G_s \end{bmatrix}$$

In this form,  $w_p$  is the matrix of performance requirements,  $w_o$  is the uncertainty bound and  $G_s$  is the plant. The matrix is turned into  $N$  via the linear fractional transformation which can be compiled using the Matlab function, lft.m using the matrix  $P$  and the controllers. The code ends with the code used to plot the robustness specifications.

Dimensions are 2x2 hence dim=2. WaSS is  $w_o$  in the code.

```
dim=2;
P=[eye(dim,dim)*0 eye(dim,dim)*0 WaSS*Gs; w_p -w_p -w_p*Gs; eye(dim,dim)
eye(dim,dim)*0 eye(dim,dim)*0; eye(dim,dim)*0 eye(dim,dim) Gs]; %creates the
generalized plant
N=lft(P,[W1*K1*Wi_2dof W1*K2]); %completes the linear fractional transformation
N=pck(N.a,N.b,N.c,N.d); %competes the packed form
Nf = frsp(N,w); %examines the frequency response over the frequency range
w
% mu for RP
blk = [2 2; 2 2]; %creates the block for the mu command
[mubnds,rowd,sens,rowp,rowg] = mu(Nf,blk,'c'); %calculates the structured singular
value
muRP = sel(mubnds,':',1); % selectes the correct structured value
pkvnorm(muRP) %computes the norm of the condition
% mu for RS
Nrs=sel(Nf,1:2,1:2);
[mubnds,rowd,sens,rowp,rowg]=mu(Nrs,[2 2],'c');
muRS = sel(mubnds,':',1);
pkvnorm(muRS)
% mu for NP (= max. singular value of Nnp)
```

```

Nnp=sel(Nf,3:4,3:4);
[mubnds,rowd,sens,rowp,rowg]=mu(Nnp,[2 2],'c');
muNP = sel(mubnds,':',1);
pkvnorm(muNP)

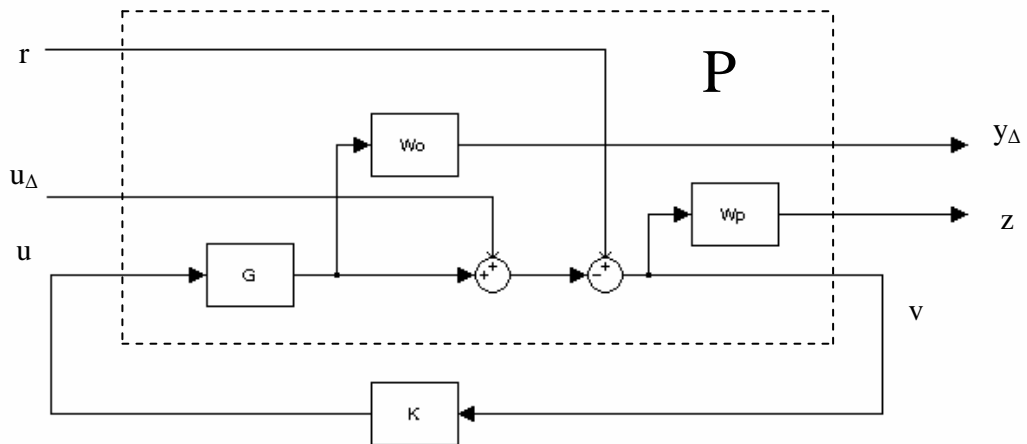
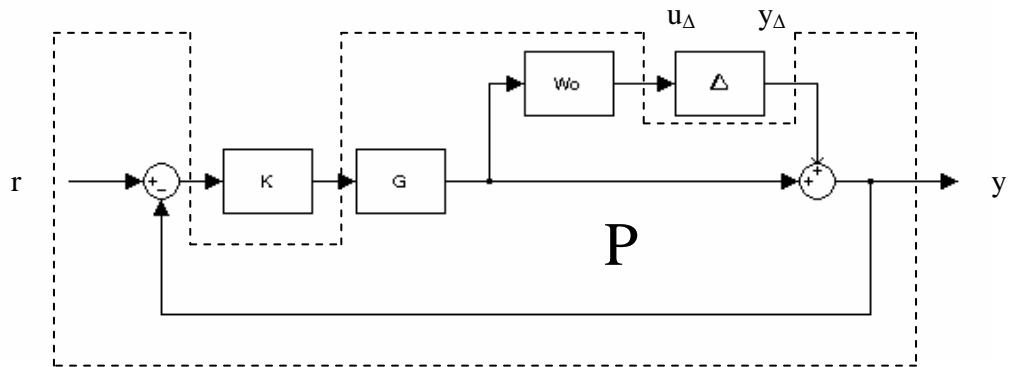
figure(1)
semilogx(muRP(1:end-1,2),muRP(1:end-1,1),'-k')
hold on
semilogx(muRS(1:end-1,2),muRS(1:end-1,1),'--b')
semilogx(muNP(1:end-1,2),muNP(1:end-1,1),'-.r')
hold off
grid, xlabel('Frequency, Hz'), ylabel('Magnitude, abs')
legend('RP','RS','NP')
title('Robustness Analysis for 2 Degree of Freedom H_{\infty}')

```

## Appendix D

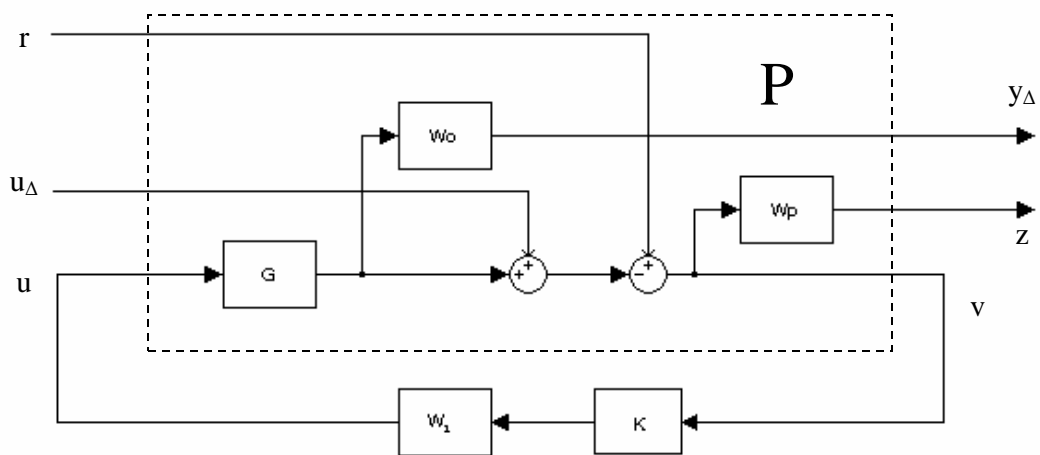
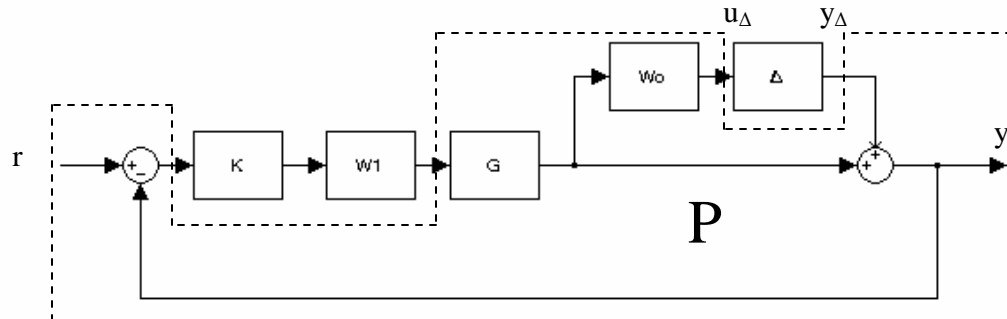
### CREATING THE GENERALIZED PLANT P FOR ROBUSTNESS ANALYSIS

#### PID/MIXED SENSITIVITY

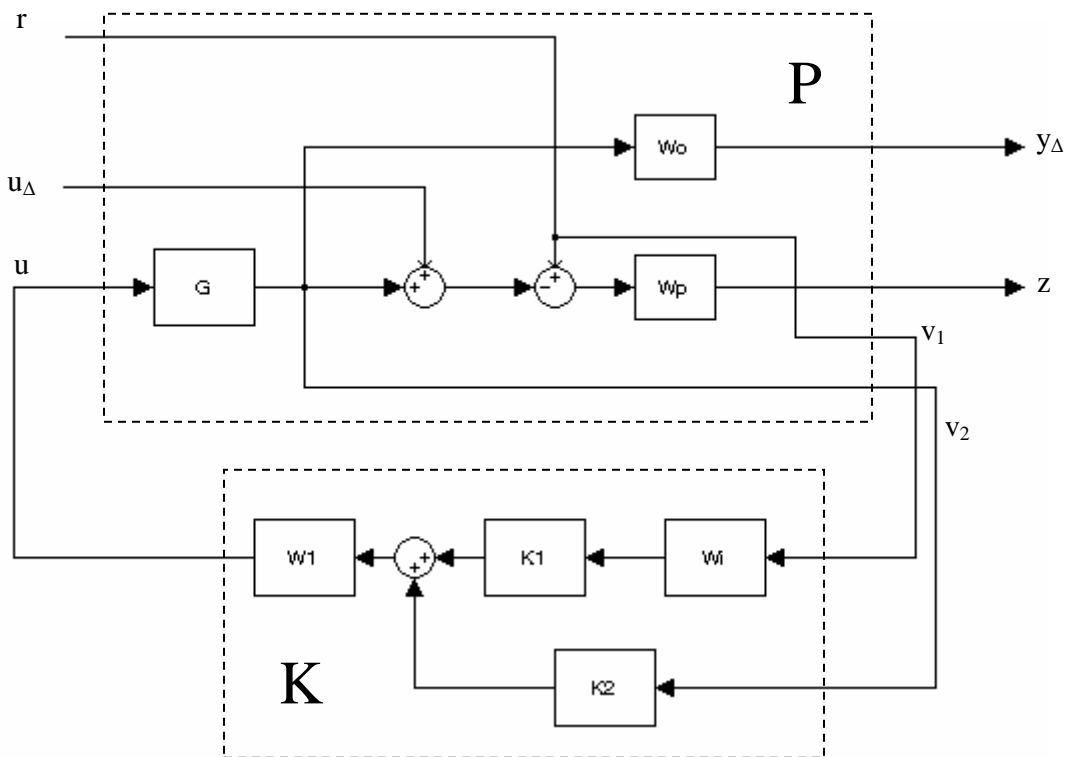
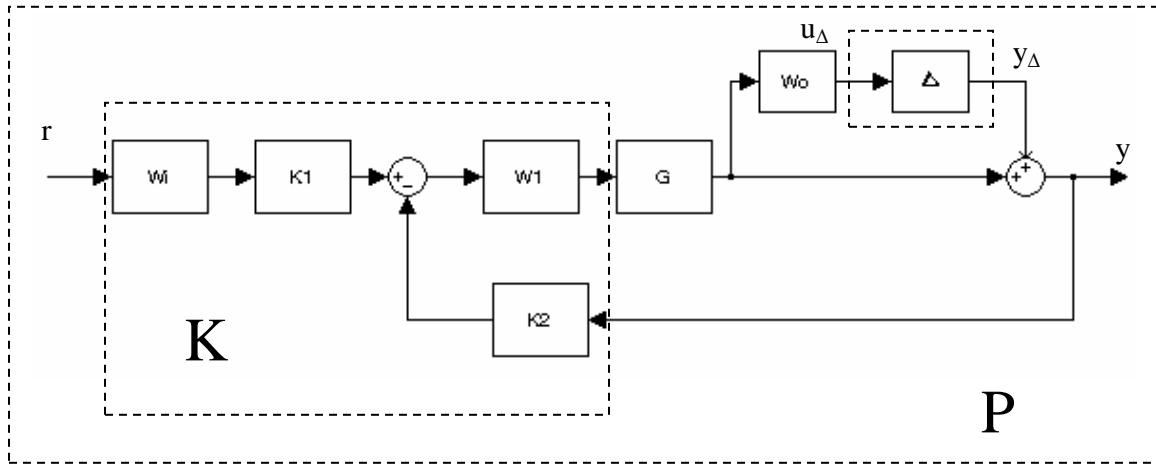




# MACFARLANE-GLOVER



## TWO DEGREES-OF-FREEDOM



## REFERENCES

- [1] Zhang, R., Alleyne, A. and Prasetyawan, E., 2002, "Modeling and  $H_2/H_\infty$  Control of an Earthmoving Vehicle Powertrain," *Journal of Dynamic Systems, Measurement, and Control*, **124**, pp. 625-636.
- [2] Skogestad, S., and Postlethwaite, I., 1996, *Multivariable Feedback Control: Analysis and Design*, John Wiley and Sons, New York.
- [3] Chen, H., Liu, Z. Y., and Sun, P. Y., 2005, "Application of Constrained  $H_\infty$  Control to Active Suspension Systems on Half-Car Models," *Journal of Dynamic Systems, Measurement, and Control*, **127**, pp 345-354.
- [4] Fales, R. C., White, W. N., and Kelkar, A. G., 1996, "A Hydraulically Actuated Compound Pendulum," *IEEE International Conference on Control Applications*, Dearborn, MI, pp. 426-431.
- [5] Fales, R. C., and White, W. N., 1999, "Control of a Double Inverted Pendulum with Hydraulic Actuation: A Case Study," *American Control Conference*, San Diego, CA, pp. 495-499.
- [6] Fales, R. C., and Kelkar, A., 2005, "Robust Control Design for a Wheel Loader Using Mixed Sensitivity  $H_\infty$  and Feedback Linearization Based Methods," *American Control Conference*, Portland, OR, pp. 4381-4386.
- [7] Manring, N. D., 2005, *Hydraulic Control Systems*, John Wiley and Sons, Hoboken, NJ.
- [8] Dean, P., Bax, B., and Fales, R., 2006, "Reliable Hydraulic Control System Design," University of Missouri – Columbia, internal document.
- [9] Balas, G. J., Doyle, J. C., Glover, K., Packard, A., and Smith, R., 1995, "hinfsyn.m," *Mu Analysis and Synthesis Toolbox, for Use with MATLAB*, Mathworks, Inc., MUSYN Inc.
- [10] Skogestad, S., 1995, "coprimeunc.m," "Matlab Files for MULTIVARIABLE FEEDBACK CONTROL."  
[http://www.nt.ntnu.no/users/skoge/book/2nd\\_edition/matlab\\_m/matfiles.html#c9](http://www.nt.ntnu.no/users/skoge/book/2nd_edition/matlab_m/matfiles.html#c9).  
April 18, 2006.
- [11] Skogestad, S., 1995, "hinf2dof.m," "Matlab Files for MULTIVARIABLE FEEDBACK CONTROL."  
[http://www.nt.ntnu.no/users/skoge/book/2nd\\_edition/matlab\\_m/matfiles.html#c9](http://www.nt.ntnu.no/users/skoge/book/2nd_edition/matlab_m/matfiles.html#c9).  
April 18, 2006.